DESIGN, CONSTRUCTION, AND TESTING OF AN OPEN-LOOP LOW-SPEED WIND TUNNEL

MUHAMMAD ADNIN BIN MAT BAHARI

UNIVERSITI MALAYSIA PAHANG

UNIVERSITI MALAYSIA PAHANG

BORANG PENGESAHAN STATUS TESIS ◆

JUDUL: DESIGN, CONSTRUCTION AND TESTING OF AN OPEN-LOOP LOW-SPEED WIND TUNNEL

SESI PENGAJIAN: 2011/2012

Saya, **MUHAMMAD ADNIN BIN MAT BAHARI (890106-06-5783)**
(HURUF BESAR)

mengaku membenarkan tesis (Sarjana Muda / ~~Sarjana / Doktor Falsafah~~)* ini disimpan di perpustakaan dengan syarat-syarat kegunaan seperti berikut:

1. Tesis ini adalah hakmilik Universiti Malaysia Pahang (UMP).
2. Perpustakaan dibenarkan membuat salinan untuk tujuan pengajian sahaja.
3. Perpustakaan dibenarkan membuat salinan tesis ini sebagai bahan pertukaran antara institusi pengajian tinggi.
4. **Sila tandakan (√)

	SULIT	(Mengandungi maklumat yang berdarjah keselamatan atau kepentingan Malaysia seperti yang termaktub di dalam AKTA RAHSIA RASMI 1972)
	TERHAD	(Mengandungi maklumat TERHAD yang telah ditentukan oleh organisasi / badan di mana penyelidikan dijalankan)
√	**TIDAK TERHAD**	

Disahkan oleh:

____________________ ____________________

(TANDATANGAN PENULIS) (TANDATANGAN PENYELIA)

Alamat Tetap:

P/S CB 3 Kg.Chatin Bukit
28400 Mentakab,
Pahang.

AHMAD BASIRUL SUBHA BIN ALIAS
(Nama Penyelia)

Tarikh: **16 JUN 2012** Tarikh: **16 JUN 2012**

CATATAN: * Potong yang tidak berkenaan.

** Jika tesis ini SULIT atau TERHAD, sila lampirkan surat daripada pihak berkuasa/organisasi berkenaan dengan menyatakan sekali tempoh tesis ini perlu dikelaskan sebagai SULIT atau TERHAD.

◆ Tesis dimaksudkan sebagai tesis bagi Ijazah Doktor Falsafah dan Sarjana secara Penyelidikan, atau disertasi bagi pengajian secara kerja kursus dan penyelidikan, atau Laporan Projek Sarjana Muda (PSM).

DESIGN, CONSTRUCTION, AND TESTING OF AN OPEN-LOOP LOW-SPEED WIND TUNNEL

MUHAMMAD ADNIN BIN MAT BAHARI

A report submitted in partial fulfilment of the requirements
for the award of the degree of
Bachelor of Mechanical Engineering

Faculty of Mechanical Engineering
UNIVERSITI MALAYSIA PAHANG

JUNE 2012

SUPERVISOR'S DECLARATION

I hereby declare that I have checked this project and in my opinion, this project is adequate in terms of scope and quality of the award of the degree of Bachelor of Mechanical Engineering with Automotive Engineering.

Signature	:
Name of Supervisor	: AHMAD BASIRUL SUBHA BIN ALIAS
Position	: LECTURER
Date	:

EXAMINER'S APPROVAL DOCUMENT

UNIVERSITI MALAYSIA PAHANG
FACULTY OF MECHANICAL ENGINEERING

I certify that the project entitled "*Design, construction and testing of an open-loop low-speed wind tunnel*" is written by *Muhammad Adnin Bin Mat Bahari*. I have examined the final copy of this project and in my opinion; it is fully adequate in terms of scope and quality of the award of the degree of Bachelor of Engineering. I herewith recommend that it be accepted in partial fulfillment of the requirements for the degree of Bachelor of Mechanical Engineering with Automotive Engineering.

Signature	:
Examiner	: MOHD FADZIL B. ABDUL RAHIM
Position	: LECTURER
Date	:

STUDENT'S DECLARATION

I hereby declare that the work in this thesis is my own except for quotations and summaries which have been duly acknowledged. The thesis has not been accepted for any degree and is not concurrently submitted for award of other degree.

Signature :
Name : MUHAMMAD ADNIN BIN MAT BAHARI
ID Number : MH08053
Date :

To my beloved father and mother:

Mr. Mat Bahari bin Abdul Ghani

Ms. Nor Ashiah binti Ismail

ACKNOWLEDGEMENTS

First of all, I want to thank The Almighty Allah S.W.T. for the beautiful life that has been given to me in the past 23 years and the present. I am very thankful to be given the time and chances to finally complete this research. I would like to express my sincere gratitude to my supervisor Mr. Ahmad Basirul Subha bin Alias for his invaluable guidance, continuous encouragement and constant support in making this research possible. He has always support me in times when I faced difficulties during completing this research and constantly giving the best advice to help me. I am always impressed with his effort in putting up with my attitude and still treated me well as his student after giving him such a difficult time. My sincere thanks go to all my lab mates and members of the staff of the Mechanical Engineering Department, UMP, who have helped me in many ways whenever I needed. Thank you for always putting up the best effort in helping me learn and familiarized myself with the equipments in the lab so that I can finish this research. The best thanks goes to my family especially to my parent, I am very thankful to have them as my father and mother because they never gave up on me and constantly support me morally and financially which are things that I needed the most in order to complete this research. But most of all, thanks for the love and attention that they gave to me which I will cherish until the end of time. Thanks for never stop believing in me although I have let them down so many times. Thanks for always pray for my success and happiness in the past, present and the future. Thanks for everything.

ABSTRACT

An open-loop low-speed wind tunnel is one of the easiest ways to study about aerodynamics for undergraduate studies. The objectives of this project are to propose a design with detail analysis, fabrication of a small scale open-loop low-speed wind tunnel and to validate the designed wind tunnel through performance testing with the existing instrumentations available in the laboratory. The wind tunnel was designed by considering the essential parts of the wind tunnel with the proper justifications before modelled with Computer Aided Design (CAD) and then tested using the Computational Fluid Dynamics (CFD). After obtaining the desired simulation result, the designed wind tunnel was fabricated and then followed by the test models. Then the wind tunnel undergoes the performance testing for validation and calibration. For the Ahmed Body flow pattern testing, the flow behaves just like the flow pattern tested in calibrated wind tunnel. For the case study testing, a cylinder model was used and the highest flow speed is 0.4317 m/s while the slowest flow speed is 0.1401 m/s. However for the case study experiment, the result obtained is not at its best condition as there is wake flow generated around the cylinder body and further improvement is required to obtain the undoubtedly results.

ABSTRAK

Terowong angin terbuka berhalaju rendah adalah salah satu daripada cara yang termudah untuk mempelajari perkara yang berkenaan dengan aerodinamik. Objektif untuk projek ini adalah untuk menghasilkan rekaan yang teliti dan membina terowong angin terbuka serta menguji keupayaan terowong angin tersebut dengan kelengkapan yang ada di makmal. Terowong angin tersebut direka dengan mengambil kira justifikasi-justifikasi yang betul pada bahagian-bahagian yang penting sebelum dimodelkan dengan *Computer Aided Design* (CAD) dan disimulasikan dengan menggunakan *Computational Fluid Dynamics* (CFD). Setelah mendapatkan keputusan simulasi yang diingini, terowong angin terus dibina dan diikuti oleh model ujian. Kemudian terowong angin tersebut diuji untuk penilaian keupayaan supaya setaraf dengan terowong angin yang telah lulus penilaian. Untuk eksperimen corak arus menggunakan *Ahmed Body,* corak arus yang diperolehi menunjukkan ciri-ciri persamaan yang ketara dengan corak arus yang diperoleh melalui model yang diuji dengan terowong angin yang ideal. Untuk kajian kes, model silinder telah digunakan dan halaju arus yang paling tinggi adalah 0.4317 m/s manakala halaju arus yang paling rendah adalah 0.1401 m/s. Walaubagaimanapun, eksperimen bagi kajian kes, bacaan-bacaan yang diperolehi adalah bukan bacaan yang terbaik kerana terdapat arus tidak stabil terhasil di sekeliling model silinder dan beberapa penambahbaikan perlu dilakukan untuk mendapatkan keputusan kajian yang tidak diragui.

TABLE OF CONTENTS

LIST OF FIGURES

.

LIST OF TABLES

LIST OF SYMBOLS

Re	Reynolds Number
V, v	Fluid velocity
D	Lateral dimension (diameter)
L	Lateral dimension (length)
υ	Kinematic viscosity of fluid
μ	Dynamic viscosity of fluid
ρ	Fluid density
El	Entrance length
Le	Length of entrance
Cr	Contraction ratio
m	meter
cm	centimeter
mm	milimeter
^{o} C	Degree Celsius

LIST OF ABBREVIATIONS

CAD	Computer-Aided Design
CFD	Computational fluid dynamic
CR	Contraction ratio
3D	3 Dimensional
2D	2 Dimensional

CHAPTER 1

INTRODUCTION

1.1 PROJECT BACKGROUND

The process for design, fabrication, and testing of an open-loop low-speed wind tunnel is discussed in this report. Important parameters in design and analysis of the small scale wind tunnel will also be presented in this chapter.

Commonly, the wind tunnel is widely used in laboratory research as well as for automotive and aeronautics industries. For instance, wind tunnel is used to enhance the performance of cars such as the new development of windshield or front bumper for better fuel efficiency and also to reduce the wind-noise. Moreover, another advantage of using wind-tunnels is the experiments can be performed under well controlled steady flow circumstances compared to experiments in the open environment. Before the wind tunnel can be used to carry out experiment, it must have instrument devices to measure the system for the wind tunnel. Generally, series of studies had been conducted in this project to make sure that the wind tunnel can carry out the experiment with the aid of several devices to be attached to the wind tunnel to come up with reliable results.

1.2 PROBLEM STATEMENT

Previously, there is no reliable small scale suction type have been developed in UMP. However, there is one discharge type wind tunnel that is available in the laboratory. But, the air flow generated inside the wind tunnel is interrupted by the fan’s blade that caused the air flow to be unsteady flow. According to aerodynamic study, the air properties are very essential in order to study the flow behaviour when it is in contact with a solid body.

1.3 PROJECT OBJECTIVE

The objectives of this project are:

(i) To propose a design, fabricate and perform detail analysis of an open-loop low-speed wind tunnel.

(ii) To validate the performance of the designed wind tunnel through the testing with the existing instrumentations available in the laboratory.

1.4 SCOPE OF STUDY

The scope of this project consists of:

(i) Detail design and analysis about an open-loop low-speed wind tunnel. The detail design consists of the justification of every essential part of the wind tunnel such as the contracting cone, honeycomb, testing section, axial fan and also the diffuser.

(ii) Computational Fluid Dynamic (CFD) to aid the designation of the wind tunnel. In this project, the CFD software used is Solidworks Flow Simulation 2011.

(iii) Validation and calibration of the designed wind tunnel using Ahmed Body and cylinder model.

CHAPTER 2

LITERATURE REVIEW

2.1 INTRODUCTION

In the nineteenth century, the astronauts to-be had studied the flight principles of the birds in order to design an aircraft. Then, humans start to make many kinds of flying machines and aviation structures. Carrying a big hope, a birdlike structure was repetitively constructed and tested in order to bring human to fly like birds. Unfortunately, the flying structure was failed each time it was tested. Soon after that, various approaches of aerodynamic studies were carried out to improvise the flying machine. Before the existence of wind tunnel, the whirling arm was used to study the air flow behavior on aircraft surfaces. The whirling arm allows people to study about the aerodynamic factors that should be emphasized in aircraft design by moving the aircraft part around in normal atmospheric condition. However, to enhance the result of the study, a better device needs to be designed. Until 1871, Frank Wenham, a Council Member of the Aeronautical Society of Great Britain, designed and operated the first wind tunnel using a steam engine powered blower fan. This first achievement of wind tunnel construction triggered a rapid development of aerodynamic study on aircraft model until now.

2.2 DESIGN OF WIND TUNNEL

In order to construct a reliable open-loop low-speed wind tunnel, the studies about designation of wind tunnels have to be carried out to avoid from making any mistakes while designing, fabricating and also testing the wind tunnel.

2.2.1 Theory of wind tunnel

According to Woodford (2011) in his journal, the basic idea of a wind tunnel is crude and simple. It is like a huge pipe that wraps around on itself in a circle or square with a fan in the middle. Then, switch on an axial fan and the air flow will flowing through it. After that, place a little door so that a model can get in a test room in the middle of the pipe and there is a wind tunnel.

In practice, it is a bit more sophisticated than that. Instead of being uniformly shaped all the way round, the pipe is wider in some places and much narrower in others. Where the pipe is narrow, the air has to speed up to get through. The narrower the pipe, the faster it has to go. It works just like a bicycle pump, where the air speeds up when you force it out through the narrow nozzle, and like a windy valley where the wind blows much harder, focused by the hills on either side.

Aerodynamicists use wind tunnels to test models of proposed aircraft. In the tunnel, the engineer can carefully control the flow conditions which affect forces on the aircraft. By making careful measurements of the forces on the model, the engineer can predict the forces on the full scale aircraft. And by using special diagnostic techniques, the engineer can understand and improve the performance of the aircraft.

Wind tunnels are designed for a specific purpose and speed range and there is a wide variety of wind tunnel types and model instrumentation. The model to be tested in the wind tunnel is placed in the test section of the tunnel. The speed in the test section is determined by the design of the tunnel. The choice of speed range affects the design of the wind tunnel due to compressibility effects.

2.2.2 Bernoulli’s principle

The relationship between the velocity and pressure effects by a moving liquid is described by the Bernoulli's principle which states that as the velocity of a fluid increases, the pressure exerted by that fluid decreases. This principle is valid for both liquid and gas. Airplanes get a part of their lift by taking advantage of Bernoulli's principle. Race cars employ this principle to keep their rear wheels on the ground while travelling at high speeds. The Continuity Equation relates the speed of a fluid moving through a pipe to the cross sectional area of the pipe. It says that as a radius of the pipe decreases the speed of fluid flow must increase and vise-versa.

In practice, for inviscid incompressible (i.e., ignoring the effects of viscosity and assuming density is constant) follow the principle of continuity and the Bernoulli equation become useful in determining average flow properties along a streamline. Time-average velocity measurements can be made with a pitot-static tube. The operation of a pitot-static tube is based upon the Bernoulli equation which for a steady incompressible flow takes the form. The Bernoulli's principle states for a fluid flowing at a certain velocity, pressure surrounding this fluid will be decreased. The explanation of the principle can be seen through its equation, the Bernoulli equation. This equation is an approximate relation between pressure, velocity and elevation. It is valid in regions of steady, incompressible flow where net frictional forces are negligible. The Bernoulli equation can be stated as:

The continuity equation is given by Equation 2.1 as below:

$$\text{AV} = \text{Constant} \rightarrow \frac{dA}{A} = -\frac{dV}{V} \tag{2.1}$$

Equation 2.1 is the continuity equation that representing the nature law of air velocity when the air flowing through a pipe or duct. The increment of the flowing area will cause the air velocity to decrease. The decrement of air velocity will occur along the increment of the passing area. In other word, the air velocity is inversely proportional to the passing area in a pipe or duct. This equation is required while designing the wind tunnel as the equation proving that the area factor is very important in designing the contracting cone and the diffuser.

Putting Bernoulli into the continuity equation given by the Equation 2.2:

$$V_m^2 = 2\left(\frac{C^2}{C^2-1}\right)\left(\frac{P_{settling} - p_m}{\rho}\right) \approx 2\left(\frac{\Delta p}{\rho}\right) \tag{2.2}$$

The Bernoulli equation can be obtained or derived by applying the conservation of linear momentum principle. The key approximation in the derivation of the Bernoulli equation is that viscous effects are negligibly small compared to inertial, gravitational and pressure effects. In theory, this fluid is called inviscid fluid.

The operation of a pitot-static tube is based upon the Bernoulli equation which for a steady incompressible flow takes the form. The Bernoulli's principle states for a fluid flowing at a certain velocity, pressure surrounding this fluid will be decreased. The explanation of the principle can be seen through its equation, the Bernoulli equation. This equation is an approximate relation between pressure, velocity and elevation. It is valid in regions of steady, incompressible flow where net frictional forces are negligible. The Bernoulli equation can be stated as Equation 2.3:

$$\frac{P}{\rho g} + \frac{v^2}{2g} + z = \text{constant} \tag{2.3}$$

Where,

$\frac{P}{\rho g}$ = static head

z = elevation

$\frac{v^2}{2g}$ = dynamic head

From that equation, the proper manner of understanding about the flow speed of wind tunnel at each point is:

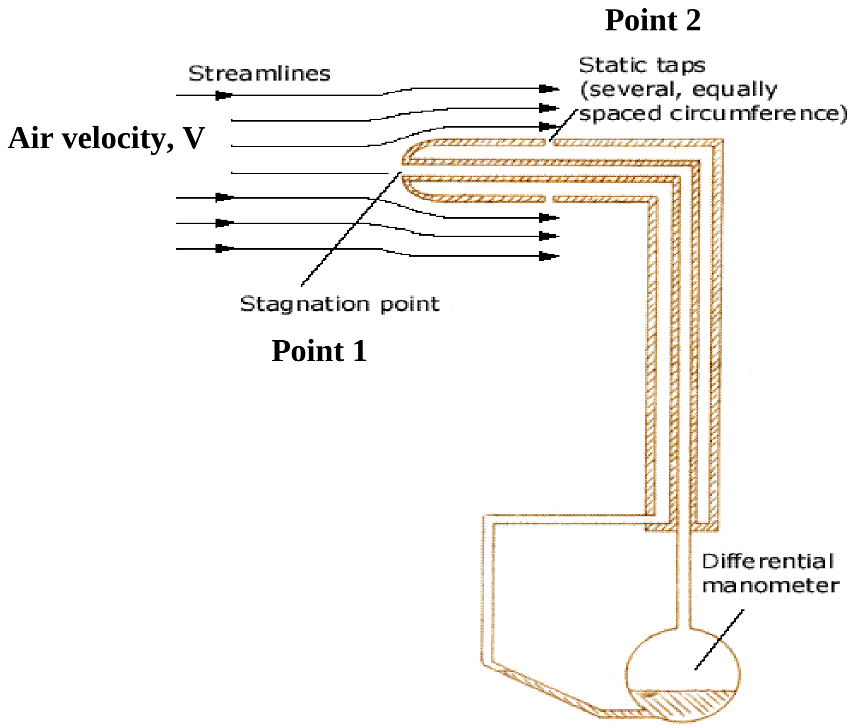

Figure 2.1: A pitot tube system

Source: Pitot, 1732

From the figure 2.1, there are Point 1 and Point 2 at in front of the pitot tube. Stagnation points exist at the surface of objects in the flow field, where the fluid is brought to rest by the object.

$$\frac{P_1}{\rho} + \frac{v_1^2}{2} + \cancel{gZ_1} = \frac{P_2}{\rho} + \cancel{\frac{v_2^2}{2}} + \cancel{gZ_2} \tag{2.4}$$

Where,

$v_2 = 0$

$Z_1 = Z_2$

$$\left(\frac{P_2 - P_1}{\rho}\right) + \left(\frac{v_2^2 - v_1^2}{2}\right) = 0 \tag{2.5}$$

From the Bernoulli's equation shows that the static pressure is highest when the velocity is zero and hence static pressure is at its maximum value at stagnation points. Hence, this static pressure is called the stagnation pressure. Point 2 is at the stagnation point where the velocity is at that point is 0. Stagnation pressure is equal to the dynamic pressure plus static pressure. Hence, the total pressure is equal to dynamic 8 pressures plus static pressure so, in incompressible flows, stagnation pressure is equal to total pressure.

The pressure at Point1 and Point 2 can be measure with using hydrostatics equation, which shown in Equation (2.6.a) and (2.6.b):

$$\text{P1} = P_{atm} + \rho g h_1; \tag{2.6.a}$$

$$\text{P2} = P_{atm} + \rho g h_2, \tag{2.6.b}$$

The Bernoulli equation could obtained or derived the by applying the conservation of linear momentum principle. The key approximation in the derivation of the Bernoulli equation is that viscous effects are negligibly small compared to inertial, gravitational and pressure effects. In theory, this fluid is called in viscid fluid.

2.2.3 Effect of flow and pressure on Bernoulli's Principal

Factor that occur the concept of Bernoulli's Principal is when the speed of a liquid or gas is low, the pressure is high, and where the speed of a liquid or gas is high, the pressure is low. Then, the speed a moving fluid or gas has an effect on the pressure exerted by the fluid decreases. As the speed of a moving liquid or gas increase, the pressure within that fluid decreases. When flow speed is at high velocity, liquid or gas trade their kinetic energy for pressure. Last factor for the drag characteristic is the faster velocities exert less pressure than slow moving velocities. (Kenneth Leet, Chia-Ming Uang. 2004).

2.2.4 Reynolds number effect

Osborne Reynolds first introduced the dimensionless constant that bears his name in his 1883, in a paper he published in the Philosophical Transactions of the Royal Society. The paper, "An Experimental Investigation Of The Circumstances Which Determine Whether Motion Of Water Shall Be Direct Or Sinuous And Of The Law Of Resistance In Parallel Channels", detailed the findings of his experimental work.

The vortex shedding from a bluff body is a function of the Reynolds Number (*Re*). The flow characteristics of wind passing across bluff body are depend on how the magnitude of inertial to viscous within the flow.

The Reynolds Number is defined as:

$$Re = \frac{VD}{\mu} \qquad \text{or} \qquad Re = \frac{\rho VL}{\mu} \tag{2.7}$$

Where,
V = the wind velocity, D or L is the lateral dimension of the body,
υ = kinematics viscosity of air,
μ = dynamic viscosity of air,
ρ = density of air

2.2.5 Wind tunnel classification

There are great deals of way to classify the wind tunnel. Several types of wind tunnel have been invented for various functions toward the study of aerodynamic. The variously types of wind tunnel are actually the evolution of the subsonic wind tunnel. Then, the existence of other wind tunnel starts to take place in aerodynamic research. Basically, the wind tunnel can be classified by its speed regime, tunnel geometry and also the working fluid in the tunnel.

2.2.6 Speed Regime

Wind tunnels are often denoted by the speed in the test section relative to the speed of sound. The ratio of the air speed to the speed of sound is called the Mach number. Tunnels are classified as subsonic ($M < 0.8$), transonic ($0.8 < M < 1.2$), supersonic ($1.2 < M < 5.0$) , or hypersonic ($M > 5.0$). The distinction of Mach number is caused by the relative importance of compressibility effects. For subsonic flows, the effects of compressibility may be neglected; for transonic and supersonic flows, compressibility effects must be considered. For hypersonic flows, we must make additional considerations for the chemical state of the gas. The scaling effects of the Mach number can be theoretically derived from the conservation of momentum of the air in the tunnel. Compressibility affects the design of the test section of a wind tunnel: for subsonic tunnels, the test section has the smallest cross-sectional area of the tunnel; for supersonic tunnels, the throat of the nozzle has the smallest area and the test section area is chosen to achieve a desired Mach number in the test section. The wind tunnels are shown in Figure 2.1(a) through 2.1(c).

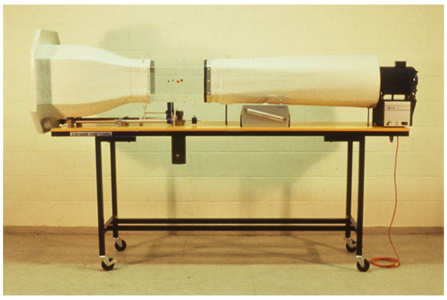

Figure 2.1(a): A subsonic wind tunnel. **Figure 2.1(b):** Supersonic wind tunnel.

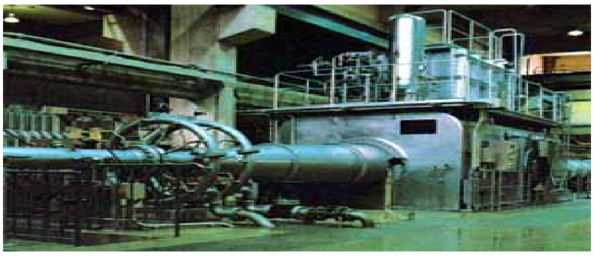

Figure 2.1(c) : A closed loop hypersonic wind tunnel.

Source: Benson, 2009

2.2.7 Tunnel Geometry

Tunnel Geometry is one of the big factors to classify the wind tunnel. Actually the wind tunnel geometry can be separated in to two sections, an open-loop and a closed-loop wind tunnel.

For an open-loop wind tunnel as shown in Figure 2.2(a), the air exhausted from the diffuser did not used back into the next cycle of the flow generation, instead, the air sucked from the contracting cone is the fresh air from the surrounding air that does not under goes any compression or heating. Tom Benson (2009) states that, “A wind tunnel that is open on both ends and draws air from the room into the test section is called an open return tunnel”. The advantages of the open-loop wind tunnel is the reduction in the cost of construction as there is no heat exchanger needed for the next cycle of flow generation. In addition, the materials used are lesser as there is no ducts construction needed to connect from the tunnel’s diffuser to its contracting cone. As for the closed-loop wind tunnel as shown in Figure 2.2(b), the geometry is very different from the open-loop wind tunnel. Closed-loop or as known as closed return wind tunnel requires a duct construction to connect the diffuser back to the entrance of the contracting cone. Heat exchanger is needed in this tunnel construction in order to reduce the air temperature to be used back in the next cycle of flow generation after the air temperature is slightly rose after being compressed by the fan.

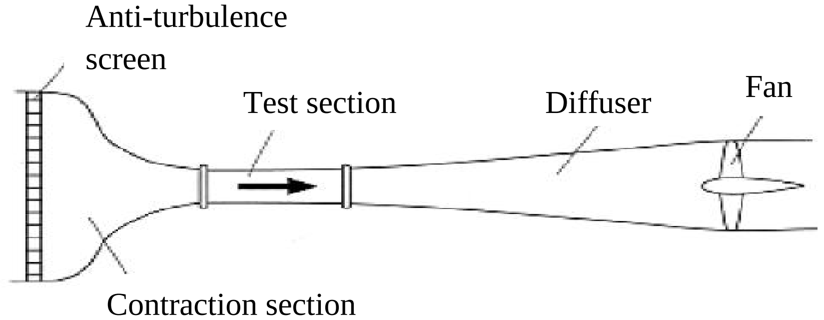

Figure 2.2(a) : A conceptual diagram of an open-loop wind tunnel.

Source: Kasravi, 2004

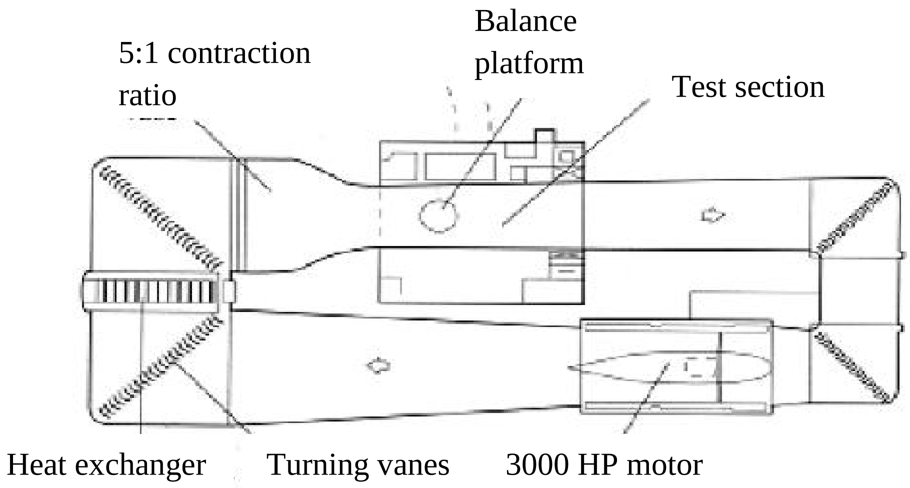

Figure 2.2(b) : A conceptual diagram of a closed-loop wind tunnel.

Source: Kasravi, 2004

2.2.8 Working Fluid

According to Tom Benson (2009), the wind tunnels can be designated by the type of fluid that is used in the tunnel. For lower speed aircraft wind tunnel testing, air moves through the tunnel. To visualize shock waves for high speed aircraft, or to study the flow around submarines or boats, water is used as the working fluid. A water tunnel is shown in Figure 2.3. In some hypersonic facilities, nitrogen or helium has been used as the working fluid. Similarly, cryogenic nitrogen has been used for high Reynold's number testing of transonic flows.

There are several wind tunnels around the world that are used to study ice build-up on aircraft parts. These icing tunnels include refrigeration devices to cool the air in the tunnel and water spray devices to provide liquid droplets in the test section.

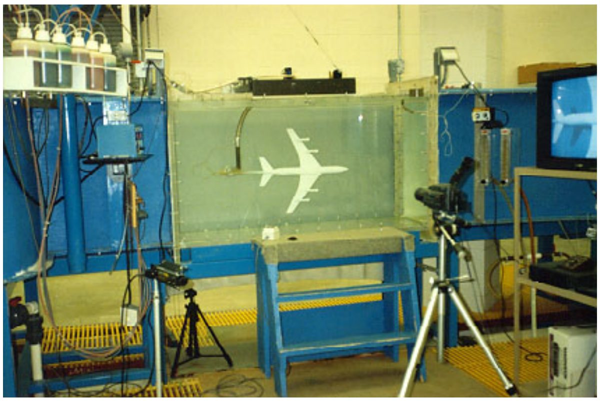

Figure 2.3 : A water tunnel to study aerodynamics in water.

Source: Anamaat, 1991

2.3 FABRICATION OF WIND TUNNEL

In order to fabricate a reliable wind tunnel, a few parameters have to be studied such as the parts that build the tunnel. Each part in the wind tunnel construction needs to be well justified so that the desired air flow generation can be accomplished. The essential parts are consisting of contracting cone, honeycomb, testing chamber or the test section and the diffuser. All these parts have its own important role before assembled to one complete wind tunnel.

2.3.1 Design parameters

Wind tunnel have two basic architecture which is open loop and closed loop as shown in Figure 2.4, according to the speed subsonic, transonic, supersonic, and hypersonic, according to the air pressure atmospheric, and variable-density, sizes small, and full-scale or air flow blower, and suction. Both types then are generally categorized in subsonic, transonic, supersonic and hypersonic wind tunnel.

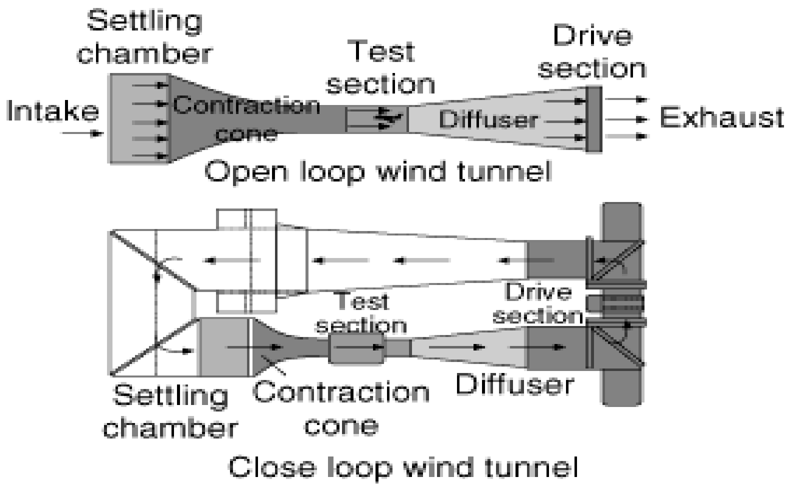

Figure 2.4 : An open-loop and close-loop wind tunnel.

Source: Dodson, 2005

2.3.2 Contraction Cone

The contraction cone's purpose is to take a large volume of low-velocity air and reduce it to a small volume of high-velocity air. The purpose of the contraction cone is to take a large volume of low-velocity air and reduce it to a small volume of high velocity air. As the air moves from the wider area of the cone into the narrower area, the speed of the air increases (Wind Tunnel, 1999).

Large contraction ratios are advantageous, contraction ratios between 6 to 9 are normally used at least for small wind tunnel. (Mehta and Bradshaw, 1979). The contracting cone ratio should be in a range of 1:6 to 1:9. The main function of the cone is actually to accelerate the air flow that sucked from the surrounding air. The ratio of the cone will exactly affects the length of the contracting cone. Several considerations need to be carried out while selecting the proper ratio for the contracting cone and the most important factor is the cost of the construction. Higher contraction ratio will cause higher cost of construction as more material needed to complete the cone.

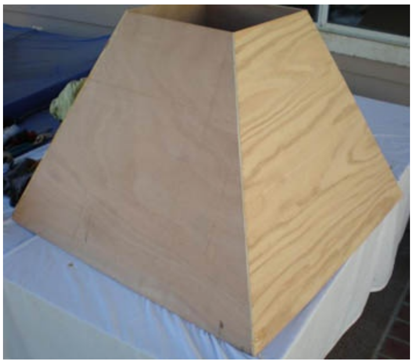

Figure 2.5 : A wooden contracting cone.

Source: Schwartz, 2002

2.3.3 Honeycomb

The settling chamber straightens the airflow. Uneven turbulent flows can cause unpredictable forces to be experienced and measured in the test section. The less turbulence there is, the better the wind tunnel will simulate actual flying conditions. The settling chamber usually includes a honeycomb flow straightener and wire mesh smoothing screens that produce a smooth airflow.

Honeycomb is effective for removing swirl and lateral mean velocity variations, as long as the yaw angles not greater than 10 degree.(Mehta and Bradshaw,1979). The honeycomb can be in circular shape, rectangular or hexagon shape. The hexagonal shape will offer higher volumetric efficiency that is preferable in the design consideration. However, the hexagonal shape is harder to be fabricated because of the complexity in shaping it. The honeycomb must at least contain 150 cells per screen and the thickness of the honeycomb must be five to ten times of its diameter.

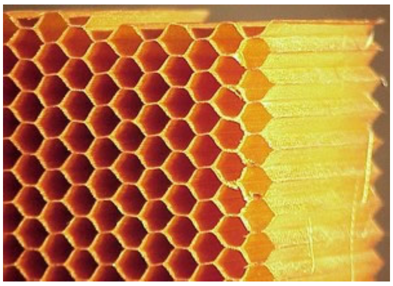

Figure 2.6 : Honeycomb (air flow straightener).

Source: Rijeka, 2005

2.3.4 Testing chamber

The test section is characterized by two properties: its size and the kind of airstream lateral boundary. The size of the test section is characterized by the cross-section of the nozzle and the length. Testing chambers in which measurements and observations are made and it was shaped and sized are largely determined by the testing requirements. (Nathan, 2009). Basically, the testing chamber dimensions are totally depends on the designer desire that actually emphasized on the fitting of the test model. The preferable testing chamber is the one that will totally fit the test model with a small distance from the honeycomb to ensure the model location is at the point which the air flow is at steady flow.

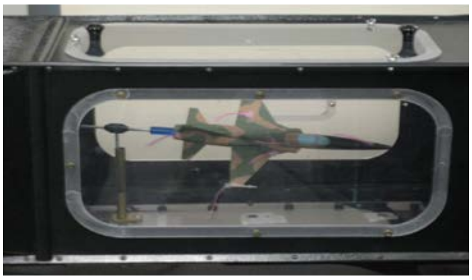

Figure 2.7 : A testing chamber of a wind tunnel.

Source: Benson, 2009

2.3.5 Diffuser

The diffuser is where the air coming out of the test section slows down prior to exhausting or reticulating. The air slows down due to the shape of the diffuser. This is an important process in the wind tunnel because it saves money. The only place where high airspeed is needed is the test section. By reducing power, the operating costs are reduced.

Diffusers are chambers that slowly expand along their length, allowing fluid pressure to increase and decreasing fluid velocity. (Nathan, 2009). The diffuser location is at another end of the wind tunnel for open-loop type. The diffuser should have rapid increment of area per distance so that the air velocity can be dropped rapidly.

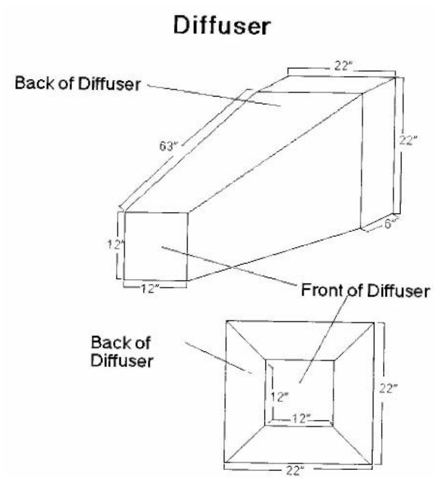

Figure 2.8: A diffuser of a wind tunnel.

Source: Dodson, 2005

2.4 TESTING OF WIND TUNNEL

To validate and calibrate the designed wind tunnel, a few testing should be made and surely with the aid of several measuring instruments that are available at the laboratory. The experimental testing take place after the wind tunnel was completed and the subject to be tested is Ahmed Body for calibration testing and a cylinder model for validation testing.

2.4.1 Ahmed Body theorem

Ahmed body is a reference body, invented by Ahmad (1984) to predict the structure of flow that passes the cars. It specially was designed to simulate the influence of the back part of the cars. The Ahmed body, shown in Figure 3.4.1, has the form of a highly simplified car, consisting of a blunt nose with rounded edges fixed onto a box-like middle section and a rear end that has an upper slanted surface (like a “hatch-back” car), the angle of which can be varied. The model is supported on circular-sectioned legs or stilts, rather than wheels. Despite neglecting a number of features of areal car (rotating wheels, rough underside, surface projections etc.) the Ahmed body generates the essential features of flow around a car, namely: flow impingement and displacement around the nose, relatively uniform flow around the middle and flow separation and wake generation at the rear. The principal aim of studying such a simplified car body is to understand the flow processes involved in drag production. Through understanding the mechanisms involved in generating drag one should be able to design a car to minimize drag and therefore minimize fuel consumption and maximize performance. The principal contribution to drag experienced by a car is pressure drag. The rear of the vehicle provides the major contribution to pressure drag and, in particular, the angle of the rear slant is critical in determining the mode of the wake flow and hence the drag experienced by the vehicle. Janssen & Hucho [135] found that the maximum drag was obtained for a vehicle with rear slant angle β 30º (to the horizontal) where the flow over the slant remained partially attached and longitudinal trailing vortices were formed at the edges of the slant. For steeper slant angles (β > 30°) the flow over the rear slant became fully-separated and the drag decreased.

Ahmed et al. observed that for a base slant angle less than 301, a separating shear layer turns up from the sides of the rear slanted edge (or C-pillar) and rolls into two longitudinal vortices. Also, the flow separates from the roof-backlight junction and then reattaches on the slant near the vertical base, forming an arch-shaped separation bubble over the backlight. Upon leaving the rear of the backlight, the flow again separates from the top and bottom edges of the vertical base, forming a large recirculatory flow region behind the vertical base. This region exhibits significant levels of flow reversal, and is characterized by two separation bubbles, one above the other and in opposing directions. Fig. 2.9 shows the proposed vortex system.

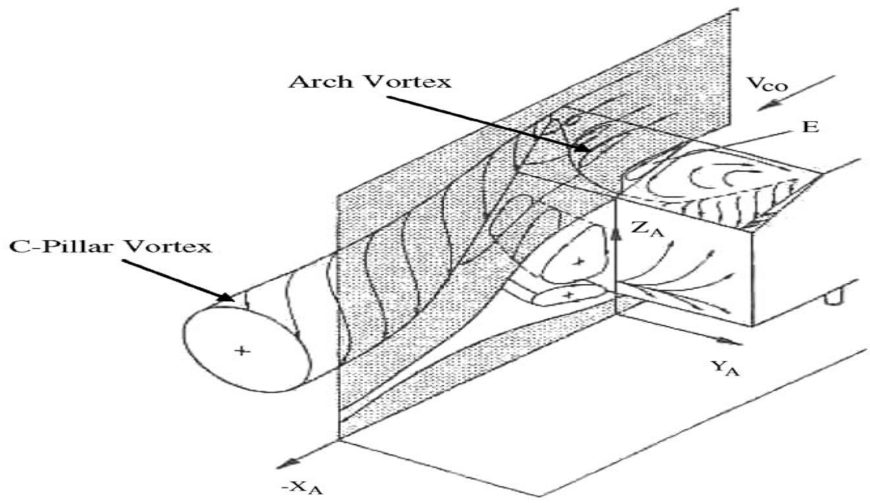

Figure 2.9: Vortex region on Ahmed Body

Source: Vino, 2004

2.4.2 Pressure Measurement

Pressure measurement is important, not only in fluid mechanics but in virtually every branch of engineering. There is a wide range of methods for measuring pressure and many of these employ hydrostatic principles. Many techniques have been developed for the measurement of pressure in testing the wind tunnel. Instruments used to measure pressure are called pressure gauges or use manometer tube. A manometer could also be referring to a pressure measuring instrument, usually limited to measuring pressures near to atmospheric. The term manometer is often used to refer specifically to liquid column hydrostatic instruments. A vacuum gauge is used to measure the pressure in a vacuum where is further divided into two subcategories which is high and low vacuum and sometimes ultra-high vacuum.

There are several types of manometer tube such as inclined, single column, U-tube, two column and two liquid types, multi-tube, portable and micro-manometer. Pressure measuring devices using liquid columns in vertical or inclined tubes are generally called manometers. One of the most common is the water filled u-tube 17 manometer used to measure pressure difference in pitot or orifices located in the airflow in air handling or ventilation system. From the figure 2.10 is the sample of multi-tube manometer at Fluid Mechanics Laboratory that have been used in the experiment.

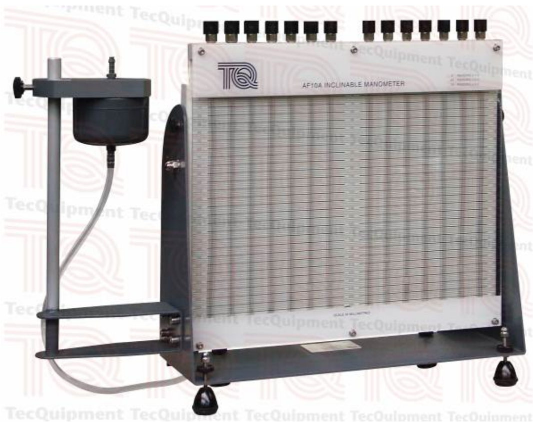

Figure 2.10: Multi-tube manometer at Fluid Mechanics Laboratory.

It can be concluded with a discussion of the units for pressure measurements. Recall that pressure is defined as the force per area. The SI unit for pressure is the Pascal, which is one Newton per square meter. For example, atmospheric pressure varies with the weather and is usually about 100 kilopascals. Common unit for measuring atmospheric pressure is mm of mercury, whose value is usually about 760 mm. In many situations, measuring pressures in units of length of the liquid in the manometer is perfectly adequate. The remainder of this document discusses how to convert from those units to Pascal.

2.5 SUMMARY

In summary, the designation of an open-loop low-speed wind tunnel must obey all the findings that discussed before but a few adjustments need to be considered in order to apply all the relevant factors into a real scale wind tunnel that to be constructed and tested. The contraction ratio must be 1:6 in order to minimize the construction cost. The honeycomb must be constructed with hexagonal cells that have the thickness of seven times of its cellar diameter. After that, the testing chamber should able to fit the test models with appropriate distance that the air for is at steady state. Finally, the diffuser must be constructed with the yaw angle is less than 10º in order to reduce the energy of the ait flow.

CHAPTER 3

METHODOLOGY

3.1 INTRODUCTION

This chapter includes the step from beginning until the end of process of performances optimization of wind tunnel using experimental method. This chapter also explains how this method applied in this project and also justify the method is suitable for this project.

3.2 PROJECT FLOW CHART

The methodology of this project needs to be closely describing the flow chart of the overall project. After the objective is set, it comes the way to setup the experiment from the early to the final stage. It is very important to ensure that there are no steps in the flow left behind or not be executed. The execution of the project must follow the flow so the project will be done smoothly without any discrepancies. The overall of the project is shown in Figure 3.1.

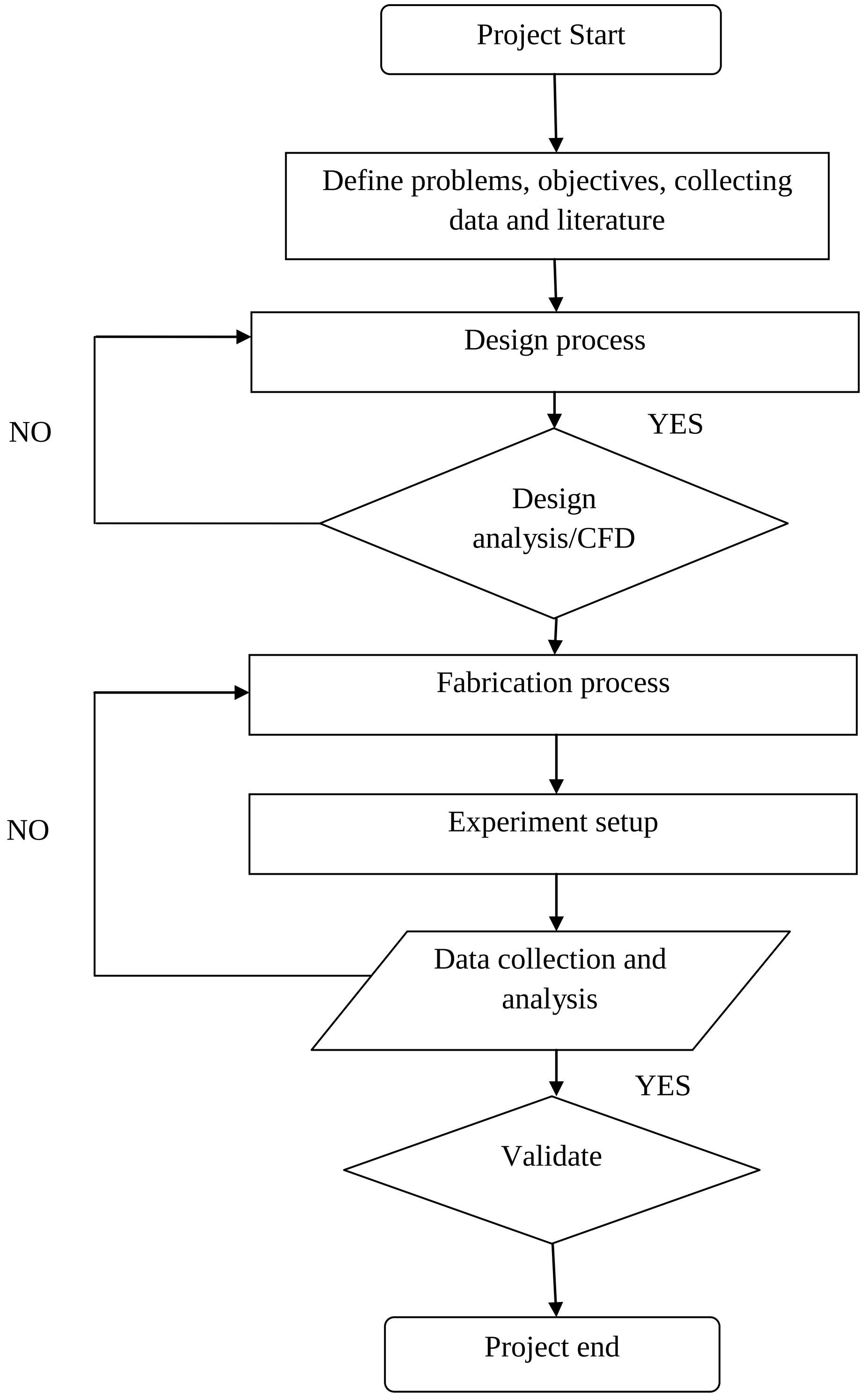

Figure 3.1: A flow chart for this project.

3.3 CONCEPTUAL STUDY

A study on the wind tunnel concept is essential for the designing a simple wind tunnel. In this conceptual study, it ought to cover basic functions in all part of the wind tunnel embodied power supply by an axial fan. To investigate and understanding the procedure of the wind tunnel is eminent in redesign the existing wind tunnel. In the present study, the works only cover the design for a reliable honeycomb or screen and test section of a wind tunnel.

Conceptual design is done to decide how the part of wind tunnel works. In this area focus on designing a reliable honeycomb, and a test section to be applied on existing wind tunnel (the parameter and dimension of a wind tunnel do not change). The new design parts are considered in order to accomplish the objectives of the project and to empower the study of vortex shedding on a bluff body.

In order to study the formation of vortex shedding on a bluff body, the length of test section part should adequately be prolonged enough to view the flow visualization at the back of a model. In case to measure the vortex shedding frequency, an unexceptional length of test section is needed because it measured by view how numerous vortices passed through a point or mark in giving the amount of time. To ascertain vortex shedding, Reynolds Number should be in more than 80.

3.4 DESIGN METHOD

There are assorted (Computer-Aided Design Aided Design) CAD software can be used in designing the 2D or 3D model such as AutoCAD, Solidworks, Solid Edge, Catia and, etc. For present study; Solidworks 2011 is applicable choose due to it fit to perform more rapidly and precise in design the model, and it is one of the most convenience software program to formulate the 3D model. On top of that, it is feasible and easier to design the complex models by design part by part of the model before assembles it.

The essential part is contracting cone that will give changes to the flow velocity if the contracting ratio changes as well. To design the most efficient wind tunnel, the contracting cone will be designed in three different ratios that are 6:1, 8:1, and 9:1 and then the best design will be chosen as the final design that can be proceed to be the part of the wind tunnel.

3.4.1 CONTRACTING CONE DESIGN

The contracting cone has to be designed based on the contraction ratio rules that is from 6:1 to 9:1. Three contracting ratios have been chosen for the design that are:

(i) Contraction ratio 6:1

This is the contracting cone with the smallest ratio in the ratio domain. So, this contracting cone will be the smallest to be compared to the other two. The dimension of this cone is represented by Figure 3.2.

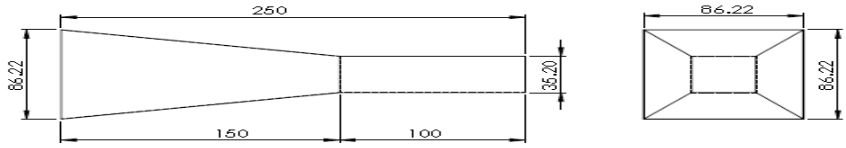

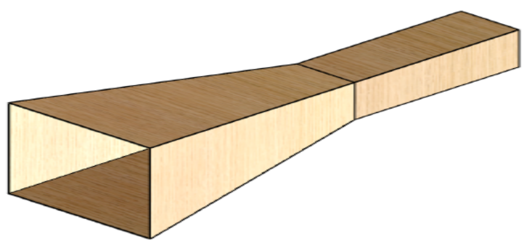

Figure 3.2: The dimension of 6:1 contracting cone in cm.

(ii) Contraction ratio 8:1

This contracting cone is to be constructed with the medium contraction ratio. This contracting cone might cause the air flow to be faster than the air flow that passing through the 6:1 contraction ratio. The materials that required building this cone are more because the size is bigger. The dimension of this contracting cone is represented by Figure 3.3.

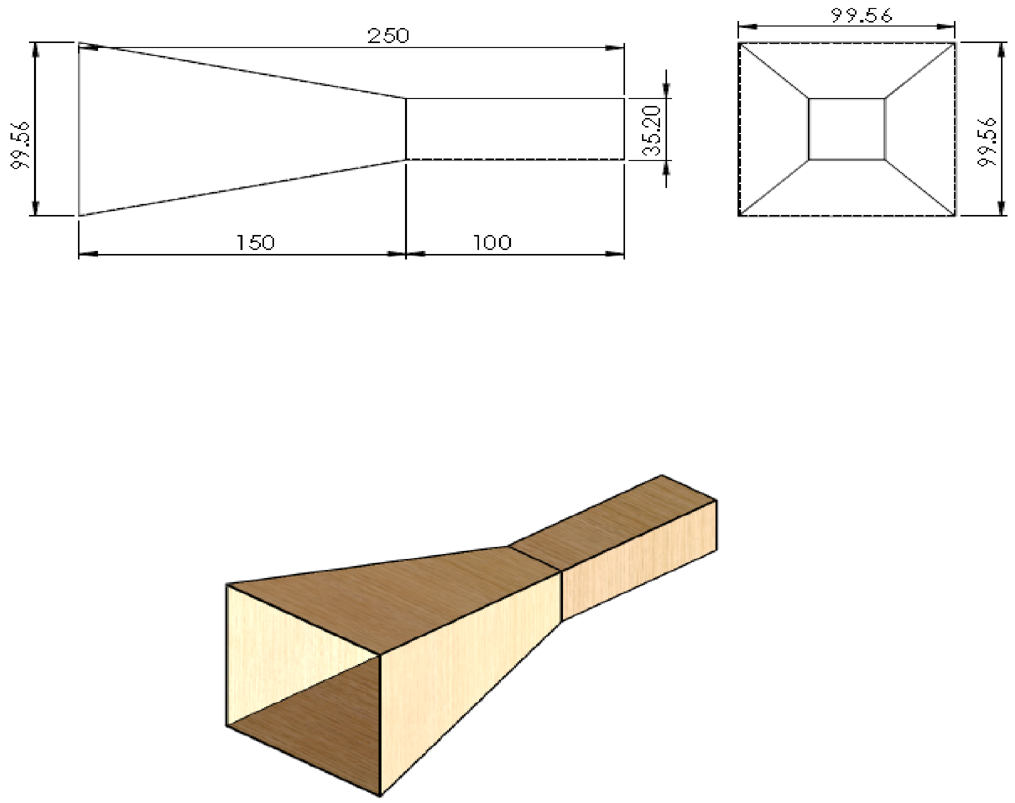

Figure 3.3: The dimension of 8:1 contracting cone in cm.

(iii) Contraction ratio 9:1

This cone is the biggest cone in size due to bigger contraction ratio. The difference between the inlet areas of this cone compared to the exhaust area is the biggest that might cause higher pressure drop and inducing faster airflow that passing through the cone. The materials required to build this cone are more that the other two because the size is the biggest to be compared to the 6:1 and 8:1 ratio cones. The dimension of this contracting cone is represented by Figure 3.4.

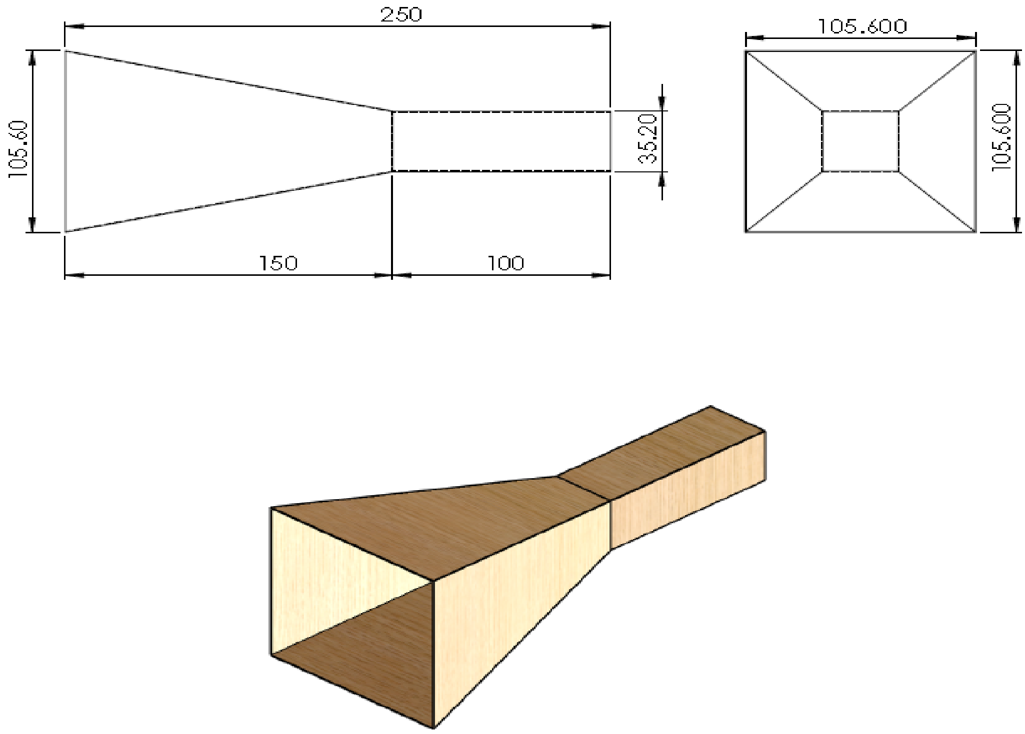

Figure 3.4: The dimension of 9:1 contracting cone in cm.

All of these three contracting cones are designed based on the contraction ratio rule from the smallest ratio to the largest ratio. The model selection is to be made by a few factors of selection such as the air flow velocity, pressure drop, and pressure distribution that to be determined by using Solidworks 2011 Flow Simulation.

3.5 DESIGN JUSTIFICATION

In the direction to guarantee the wind tunnel to works according to the needful performance, series of calculations need to be organized as the design justification of every prominent part of the wind tunnel. A number of calculations must be considered during the design stage and shown as the listed below:

3.5.1 Item to be considered:

(i) Contracting cone dimensions

3.5.2 Contracting cone dimensions

In this project, the contracting cone dimensions were determined by obeying two rules of cone length selection that stated as below:

(i) Entrance length formula, El
(ii) Contraction ratio, CR

3.5.3 Entrance length formula, El

The first rule of cone length selection determined by calculating the Reynolds Number of the air flow that entering the contracting cone. Then after the Reynolds Number was determined whether it is laminar or turbulent, the Reynolds Number then inserted into the Entrance Length equation to obtain the maximum required entrance length of the contracting cone.

The sample calculation:

Assumptions:

(i) The study is conducted at 25 ºC of the room temperature.

(ii) The fan speed is at normal state of 2.0 m/s of the air velocity.

(iii) The pressure is 1 atm of normal room condition.

Reynolds Number:

$$\text{Re} = \frac{\rho \upsilon d_h}{\mu} \tag{3.1}$$

Where,

Re = Reynolds Number (to be determined)

ρ = air density, kg/m^3

υ = air velocity, m/s

d_h = hydraulic diameter of the contracting cone (duct), m

μ = absolute viscosity of air, cp

At 25 ºC,

ρ = 1.1845 kg/m^3

$\upsilon = 2.0$ m/s

$d_h = 1.23$ m

$\mu = 0.01827$

So,

$$\text{Re} = \frac{(1.1845 \text{ X } 2.0 \text{ X } 1.23)}{(0.01827)}$$

Thus, Re = 160 , is laminar.

For laminar value of Reynolds Number, The entrance length formula is

$$\text{El Laminar} = 0.06 \text{ Re} \tag{3.2}$$

Thus, El Laminar = 0.06 (160)

= 9.6

Then the entrance length value is inserted in Length of Entrance formula.

$$\text{Le} = \frac{El\ Laminar}{d_h} \tag{3.3}$$

Thus, $\text{Le} = \dfrac{9.6}{1.23}$

$= 7.8$ m

Therefore, the maximum required length of the contracting cone is 7.8 m.

3.5.4 Contraction ratio, c

Based on the findings in the literature review, the required contraction ratio, c is at least 1: 6 for small scale wind tunnel. According to Mehta (1979), “Large contraction ratios are advantageous, contraction ratios between 6 to 9 are normally used at least for small wind tunnel”. So, the contracting ratio for this wind tunnel is 6 to minimize the cost of construction.

Calculation:

In this project, the exhaust width and length of the contracting cone is known to be the same as the width and length of the exhaust fan which is both 35.2 cm. So, the area of the exhaust of the contracting cone can be calculated as:

$$\text{Area} = a \times b \tag{3.4}$$

Where:

a = width of the exhaust of the contracting cone.

b = length of the exhaust of the contracting cone.

Area = 35.2 cm x 35.2 cm

= 0.127 m^2

So, the exhaust area is 0.127 m^2. Then, according to literature review, the cone ratio should be 6 that mean the inlet cone area is six times larger than the exhaust area. The inlet area of the cone can be calculated as:

0.127 x 6 = 0.762 m^2

Since the area is square, then the inlet area value is to be square root of two to determine the length and width of the inlet of the cone.

$\sqrt{0.762}$ = 0.874 m, so, both length and width of the cone inlet is 0.874 m.

3.6 DESIGN ANALYSIS

In this manner, the designed wind tunnel including the honeycomb and test section is analyzed by applying the CFD software. The software that was used for the analysis is COSMOS Floworks 2011.

The investigation is focused on new design of honeycomb and test section part. The air flow characteristic (laminar or turbulence flow) passes through the wind tunnel are discussed. This analysis is to foretell the moving flow around the bluff model in the investigation.

3.7 MODEL SELECTION

There are only two sets of models that will be tested, that are Ahmed Body and cylinder model. The parameter and dimension of the models are shown in below.

3.7.1 Ahmed Body

The model will be designed and developed in tiny scale due to a small area of the wind tunnel. The scale is 1/4 from its original parameters, and the full-scale dimension of 1/4 is displayed in Figure 3.6 below.

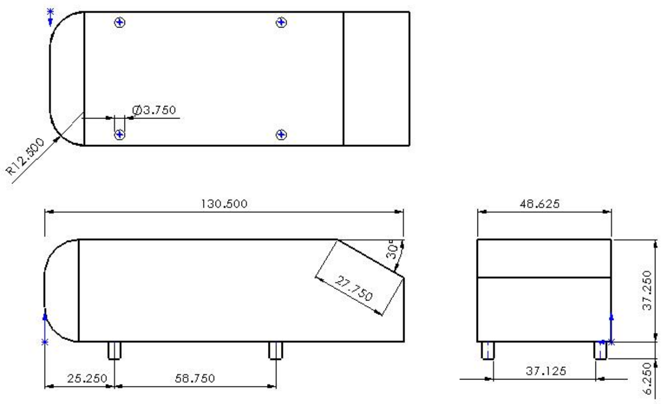

Figure 3.5: The dimension of Ahmed Body model, all dimensions in mm

3.7.2 Case study: Cylinder

A cylinder model has chosen as a model of a case study in this project. The cylinder is made of aluminium sheet with a diameter 11.0 cm. The numerous manometers are used for all pressure measurements. There are eight tubes are connected to the manometer. Take best to take an average of these for the static pressure. The manometer is used to measure the static pressure. The manometer should be tilted to its inclination of 45°. The density of the fluid in the manometer is 0.79 $g.cm^{-3}$. There were eight tubes attached to the cylinder.

3.8 FABRICATION PROCESS

In this part, the fabrication processes of the wind tunnel and all the models are to be discussed. All of the justifications were applied while constructing the wind tunnel. For the scaled-down test model, the geometries are all identical with the exact dimension model.

3.8.1 Wind tunnel

Firstly, the construction of the wind tunnel is to be discussed; the essential parts such as contracting cone, honeycomb, testing chamber and diffuser are constructed based on the justification as shown in Figure 3.6(a). The majority of the wind tunnel body's are made of wood such as the contracting cone and diffuser. The main reason of the usage of the wood is the ease of shaping because the wood is a lot easier to be cut using a hand grinder. Moreover, the wood are cheaper if to be bought in huge amount, so it was preferable than using the steel sheets.

The wooden cone then joined by the 1/4 inch x 2 inch wood frame. To attach the wooden cone to the wooden frame, three-quarter inch screws are used because to ensure higher attaching strength than using nails and the screws are preferable when the disassembling action is needed while doing the construction. To ensure that there is no air flow leakage at the wooden parts, the silicone glue was used as a sealant at the suspected area of easier leakage such as at the joint areas.

Next, as for the honeycomb, the selected design is the hexagonal cellar shape because it offers better uniformity of the cells and it offers higher volumetric efficiency than the circular or rectangular shape. The honeycomb is fully made of hard cover paper. The main reason of the paper selection as the main material is the cost of construction and the ease of shaping. The paper is very cheap to be compared to other material but the durability is not good. Considering the honeycomb will not undergoes any heavy-duty tasking, and then the paper would be a great choice. Each cell is at about 6.0 cm of perimeter and at average of 2.0 cm of diameter. The cells are folded one by one until the area of 35.7 cm x 35.7 cm is fully covered. To fully covered, 329 cells are required to be attached together as a honeycomb. The installed honeycomb is shown in Figure 3.6(c).

After that, the testing chamber as in Figure 3.6(b), was fully made of Perspex or as known as Polymethyl Acrylic. The reasons of using the Perspex are the ability of the perspex that known as transparency, light weight and also cheap. Transparency is preferable in this construction because the only way to calibrate the wind tunnel is by conducting the flow pattern test. The Perspex was cut using the special Perspex knife first, and then, after the required length and width were acquired, the Perspex sheets then joined to be a rectangular duct using the hot candle glue and next the silicone glue was applied at the joint parts as a sealant for any air flow leakage.

For the blower fan, firstly the fan is placed in the testing section and then was pushed at the very end of the testing section duct. After that, the fan was fixed using the hot glue gun and then the silicone sealant was applied as well.

All the parts are assembled to be a completed wind tunnel. The contracting cone, honeycomb, testing chamber, blower fan and also the diffuser were arranged in the right order properly. Then, to carry out the experiment, a 3.0 cm diameter hole drilled at the bottom-center surface of the testing chamber as an opening for the hot wire anemometer sensor as shown Figure 3.6(e) and the smoke generator outlet to be put inside the testing chamber.

Figure 3.6(a) : A completed wind tunnel.

Figure 3.6(b) : A testing chamber.

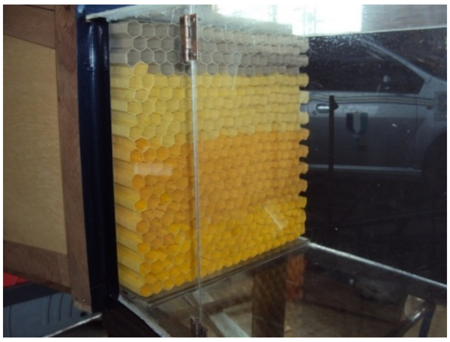

Figure 3.6(c) : A honeycomb (329 cells).

Figure 3.6(d) : An axial exhaust fan.

Figure 3.6(e) : A set of a hot-wire anemometer.

3.8.2 Position of model testing

The model is placed at the center of the test section center line of the leading edge of the inlet of the test section. The model is positioned horizontally with the model's leg or stand which is located at bottom surface of the test section and was set to fix. The model is located such that the air flow or vortices at the back of the body will get to be stable and uniform before it's scattered at the outlet of the test section. The model positioning is shown in Figure 3.7(a) and 3.7(b).

Figure 3.7(a) : A side view of the model.

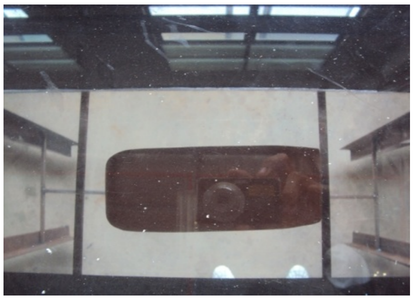

Figure 3.7(b) : A top view of the model.

3.8.3 Position of smoke generator outlet

The emplacement of the smoke generator is foremost to make sure well-behaved flow visualization is attained. The smoke generator outlet is positioned at 10.0cm from the top edge of the model, and the length is 30.0cm from the model. The exhaust outlet is located such that its wake would not obstruct with the flow around the model.

3.9 EXPERIMENTAL TECHNIQUE

For the experimental of vortex shedding around Ahmed body, the tests were performed at Reynolds Number above 80 which are the criteria to investigate of vortex shedding. The Reynolds Number ranges are based on the chord length, L of Ahmed body by varied the speed fan. The model was performed in two sets of experiment by vary the Reynolds Number according to the fan speed. In the first set of experiment, the fan speed is set to 0.6 m/s. For the second set of experiment is set the fan speed to 2.0m/s.

The sensor of the hot wire anemometer is located at the center region inside of the inlet test section as shown in Figure 3.8. The velocity is measured when the value becomes stable and means velocity is calculated before all set of experiment is performed. All the test was conducted in three experiments before the averages were calculated and analyzed.

Figure 3.8: An anemometer sensor inside the test section

In the smoke visualization method, the digital camera is used for capturing the flow at instantaneous time. The camera is located at side view (for analysis of smoke pattern on the front part, slant surface and vertical base) and at rear view, behind of the model (for analysis of counter rotating vortex). The location of the camera behind the model is 500mm so the flow behind the body will fully developed and does not interfere with the camera. Meanwhile, for the analysis of vortex on curved part the short video is captured. All the experiment is conducted in dark room with support by flash lighting to view the smoke flow.

3.10 SIMULATION TECHNIQUE

The present configuration of simulation is used COSMOSFloworks 2011 software. The Ahmed body is design using Solidworks before export to Floworks. For the analysis type, external flows analyses deal with flows over or around a model and both cavities without flow conditions and internal flow is applied and all physical features such as gravitation, rotation and radiation is ignored. Air is used as fluid domain and laminar and turbulence flow is set.

For the computational domain, the size of the rear part or outflow is 0.6m, extends to 5 times of body lengths. This consideration is applied to make sure that the outlet flow condition does not affect the near-body wake (Rodi, 2004). The inlet flow is placed at 0.17m from front part (1.5 of body length), both width and height is set 5 body lengths corresponding to 0.2m and 0.19m. At the inflow section, a uniform velocity is applied and turbulence intensity is set 1.8% with turbulence length of 0.0005m. At both side boundaries and the top and bottom boundaries, free-slip conditions are applied as in Figure 3.9.

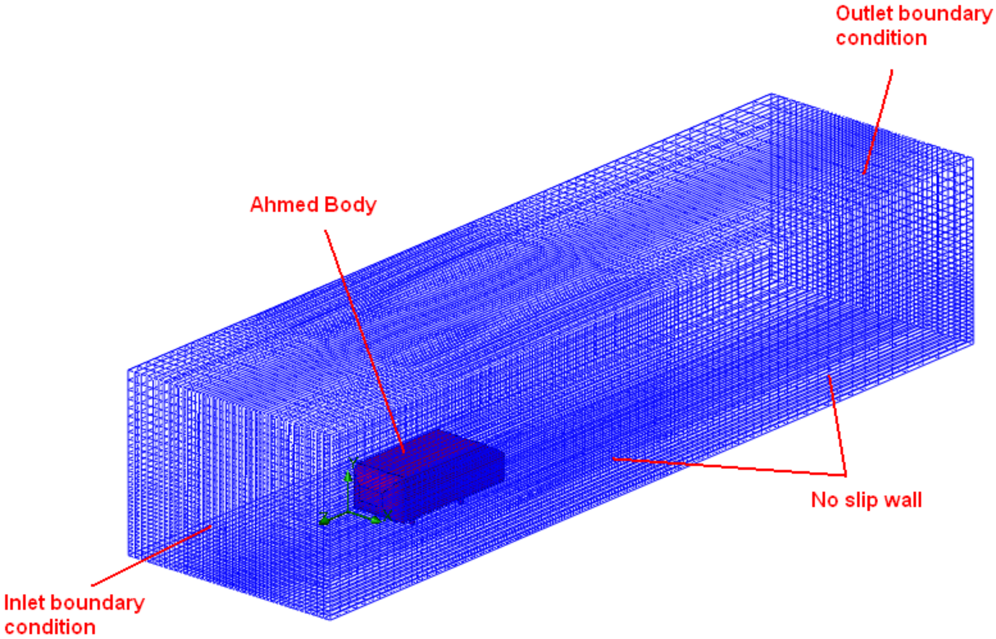

Figure 3.9: Computational domain and boundary condition

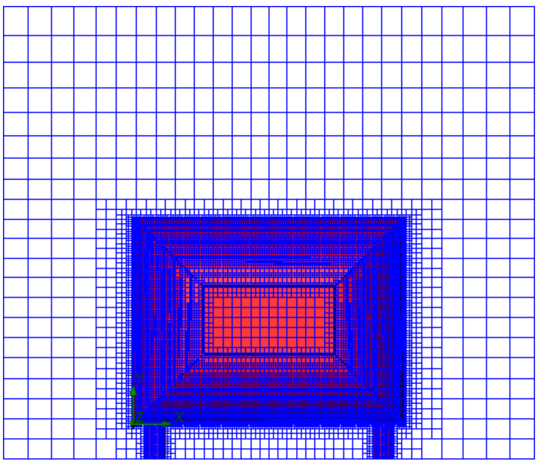

(a) Front view

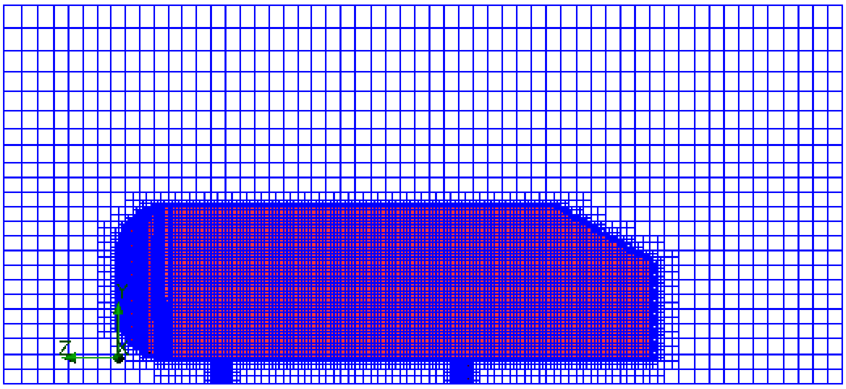

(b) Side view

Figure 3.10: Grid refinement around the Ahmed body model

Figure 3.10 shows meshing of computational domain and grid refinement of the model. In grid or meshing part, 46 blocks (x-axis), 32 blocks (y-axis) and 106 blocks (y-axis) is set for the computational domain. The grid refinement is applied on bluff model by using the initial mesh condition. The small solid features is set to level 4, for curvature refinement is set to level 5 and level 3 is set for the tolerance refinement. For fluid and partial refinement cells, both are set to level 4 and level 2. Meanwhile, the number of cells across a narrow channel is 70 with narrow refinement is 3. The overall meshing shows the number of cells is 392968, fluid cells 243650, solid cells 67327 and partial cells is 81991.

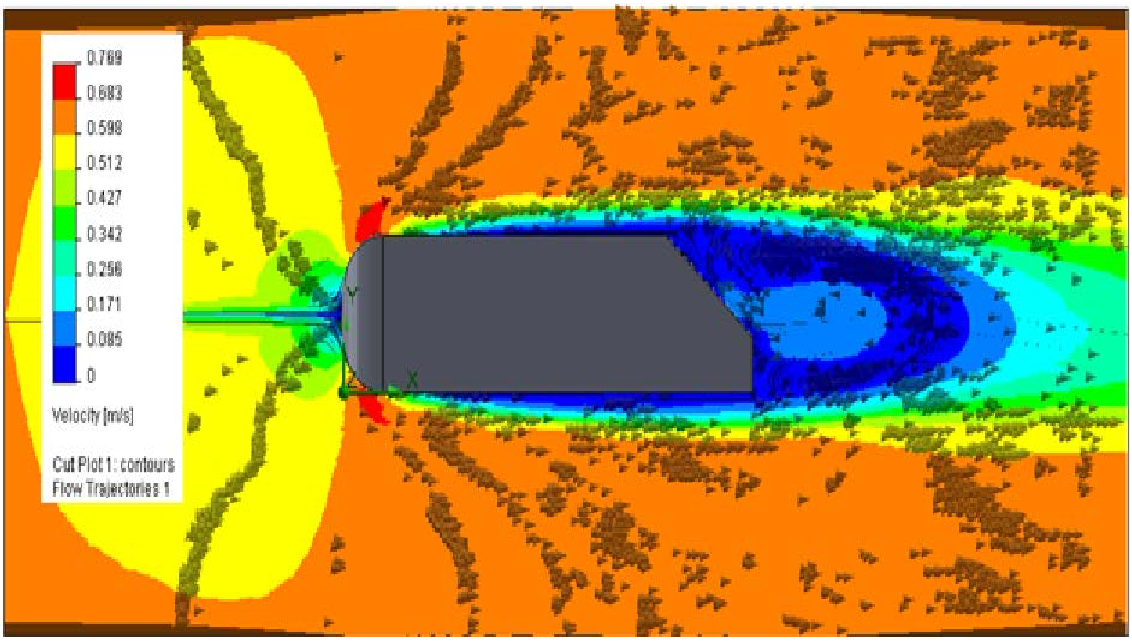

Figure 3.11: A velocity testing using Solidworks 2011 Flow Simulation.

Figure 3.11 shows the flow simulation when an air flow of 0.6 m/s in velocity was in contact with Ahmed Body. The flow trajectory is in velocity profile and the velocity distributions are different at different spots. From the figure, the highest velocity is at about 0.769 m/s and it is at the starting of the increasing of the frontal area of the Ahmed body. Meanwhile, the slowest air velocity is at 0 m/s at two spots which are at the front point of the model that known as stagnation point and at the back of the model that known as wake region. The stagnation point is where the air flow is damped when the trajectories is about to hit the frontal area of the model, the air flow might be damped to be at 0-0.171 m/s. Meanwhile at the wake region, the air flow that flow through the model become unstable and starts to interrupt each other. In this region, the flow separation is predicted to happen for the real testing where there are two type of flow pattern might happen at this region.

CHAPTER 4

RESULTS AND DISCUSSION

4.1 INTRODUCTION

This chapter will discuss on the result of the fabricated wind tunnel performance, a case study of the cylindrical model. The pressure difference at the cylinder surface model will be discussed including the calculation between the flow speeds on the model's surface and also the drag coefficient. In addition, this chapter will also discuss about the observation of characteristic of the smoke pattern around Ahmed Body. Then, the experimental result will be compared with the CFD simulation results.

4.2 SELECTION OF CONTRACTING CONE

4.2.1 Contracting Cone

To select the best contracting cone for the wind tunnel design, a series of flow simulation tests have to be done to determine the air flow condition inside the contracting cone. From Figure 4.1.a) through Figure 4.1 b), there are three points to be determined the pressure and velocity of the air flow. The air flow speed can be measured at the three points then to be compared with the other two model of contracting cone. Then, the pressure drop or pressure difference can be determined by subtracting the pressure value at Point 1 to the pressure value at Point 3. The points represent the three areas inside the contracting cone which are Point 1 represents the inlet area, Point 2 represents the middle area and Point 3 that represents the outlet area of the contracting cone that was attached together with the testing chamber. The initial velocity of the air induced inside each cone is 2.0 m/s.

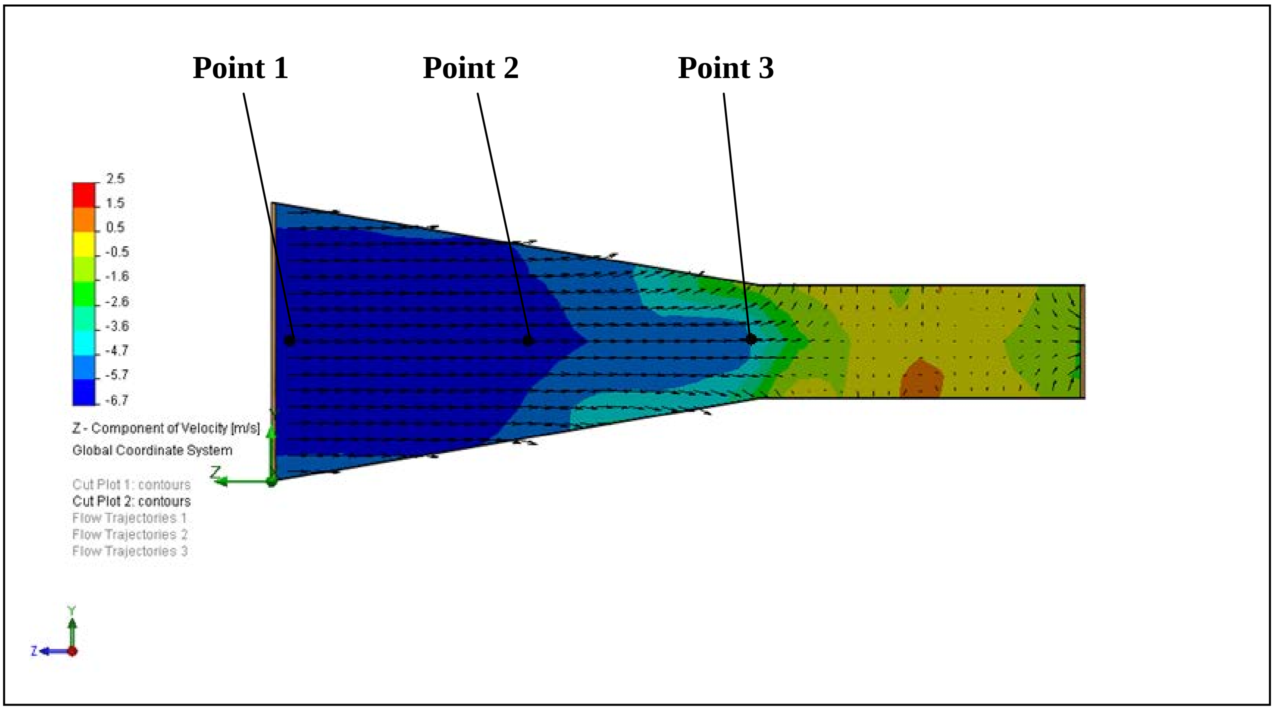

Figure 4.1(a): Air flow speed simulation for 6:1 contracting cone

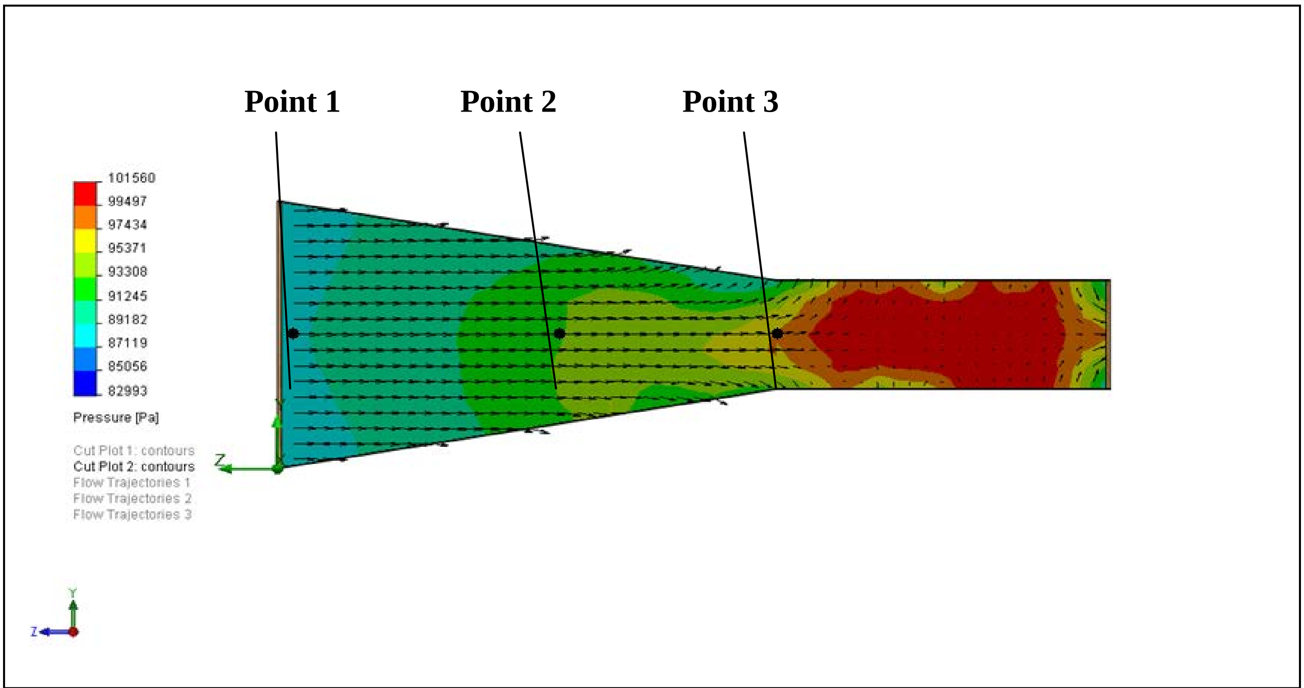

Figure 4.1(b): Air flow pressure simulation for 6:1 contracting cone

Both air flow pressure and air flow speed are indicated by the cutplot with various colours to differentiate the contour. Different colour means different value of the measured parameters. The other contracting cones are also tested with the simulation in order to accumulate the data at those three points. The data is represented by Table 4.1.

Parameters	**CR 6:1**			**CR 8:1**			**CR 9:1**		
	Point 1	**Point 2**	**Point 3**	**Point 1**	**Point 2**	**Point 3**	**Point 1**	**Point 2**	**Point 3**
Flow speed, m/s	6.7	6.7	5.7	6.7	6.7	6.7	6.1	6.1	6.1
Pressure, Pa	87119	91245	95371	83284	83284	85316	99677	99677	99677

Table 4.1: Air flow speed and pressure distribution for 6:1, 8:1 and 9:1 cone

Table 4.1 shows the data about air flow speed and pressure distribution at three selected points for 6:1, 8:1 and 9:1 contracting cone. This data is accumulated to study the air flow condition inside the contracting cone with different contraction ratio, CR. With the obtained data, the selection of the contracting cone can be made without doubt because the pressure distribution and the air flow velocity range of all three cones are known. For further understanding of this data distribution, the data can be represented by a graph at Figure 4.2.a) and Figure 4.2.b).

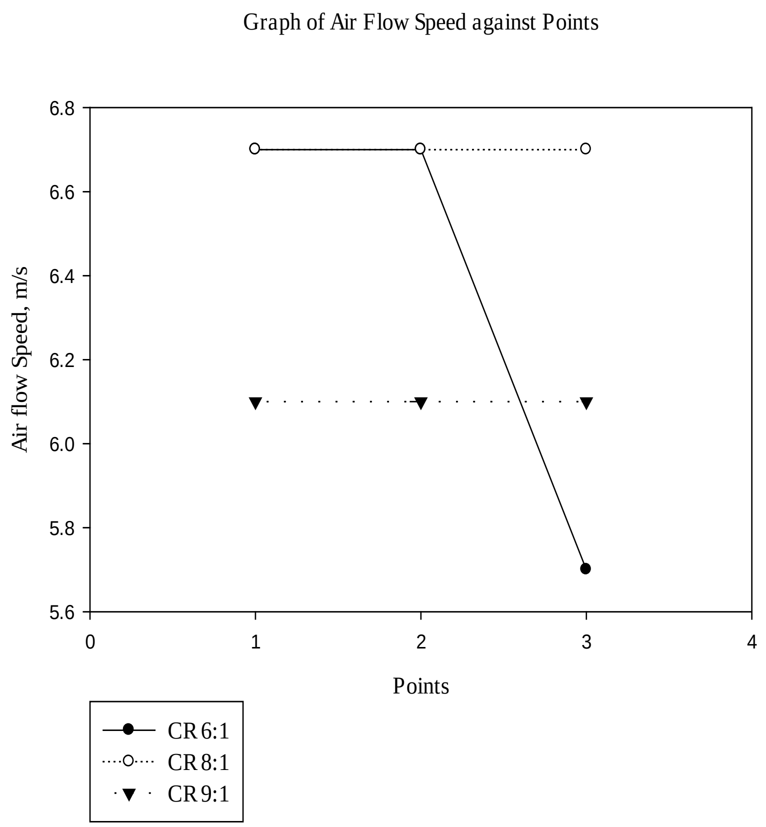

Figure 4.2.(a): Graph of Air Flow Speed against Points

Figure 4.2.(a) indicates the effects of the contraction ratio upon the air flow speed when the air passes through the contracting cone. From the graph, at Point 1, the highest air flow speed goes to 6:1 and 8:1 cones that measured with 6.7 m/s while 9:1 cone induce the slowest air flow speed with 6.1 m/s. This is because the 6:1 and 8:1 cones have smaller inlet area to be compared to the 9:1 cone. Higher area means higher volume and higher mass to be move at the same pressure. So, a higher power fan is needed to pull a huge volume of air at the inlet area of 9:1 cone. At Point 2, the air speed for 6:1 and 9:1 cones air speed remains the same and the air speed for 8:1 cone starts to drop. This might due to the momentum of the air flow, the air speed for 6:1 cone remains to be faster because of the smaller sum of the air volume to be moved while the air speed for 9:1 cone remains to be slower because of the higher sum of air volume have to be moved by the same power blower fan. For 8:1 cone, the air speed slightly dropped due to the damping of the air flow as the area of the ducts become smaller. At point 3, the duct become at its smallest area, there is no change in air flow

speed for 6:1 and 9:1 cone because of the same ratio of increment of the air volume to the passing area with the same fan power. For 8:1 cone, the air speed finally drops to 5.7 m/s because of the flow damping. According to Bernoulli's continuity equation, the air flow speed should constantly increase along with the reducing passing area. For this case, the air speed velocity did not obey the principle and it is probably because of the low fan speed to pull the air through the cone.

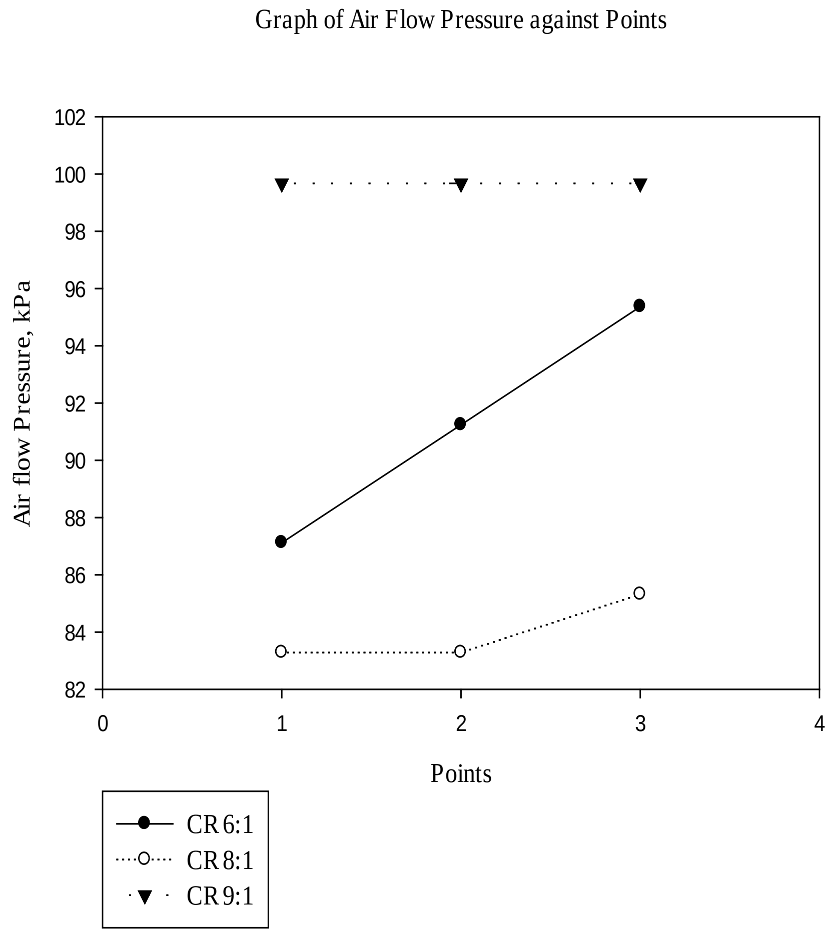

Figure 4.2.(b): Graph of Air Flow Pressure against Points

Figure 4.2(b) indicates the air flow pressure distribution at each point that selected to be studied when the air flow passing through the contracting cones. From the graph, the pressure distributions for 6:1 and 8:1cones are increasing from Point 1 through Point 3 from 87119 Pa to 95371 Pa and from 83284 Pa to 85316 Pa consequently. This is due to compressibility factor of the air that might increase when moving from larger to narrower space forced by the blower fan. When the air compressed under a little compression, the density at that certain area will be slightly increased and then followed by the increasing of pressure. For 9:1 cone, the pressure distributions are not giving any changes from Point 1 to Point 3. The pressures are uniform although the space is getting narrower. This phenomenon might happen due to the sufficient space for the air to uniformly flow through the cone and also insufficient power to compress the air by the fan. The pressure difference inside every cone can be calculated by subtracting the pressure value at Point 3 with the pressure value at the very inlet of the cone which is the pressure value at Point 1. The pressure difference inside every cone is represented by Table 4.2.

Parameter	CR 6:1	CR 8:1	CR 9:1
Pressure difference, ΔP, Pa	8252	2032	0

Table 4.2: Table of pressure difference inside contracting cones

From 4.2, there are only positive difference occurred inside each cone except for 9:1 cone that comes out with no difference in pressure. The positive difference means along with the narrower area, the pressure is slightly increasing due to a little compression before the air is naturally allowed to pass through the cone into the testing chamber and finally exited through the diffuser. The pressure difference for 6:1 cone is 8252 Pa and for 8:1 cone is 2032 Pa consequently.

4.2.2 Testing Chamber

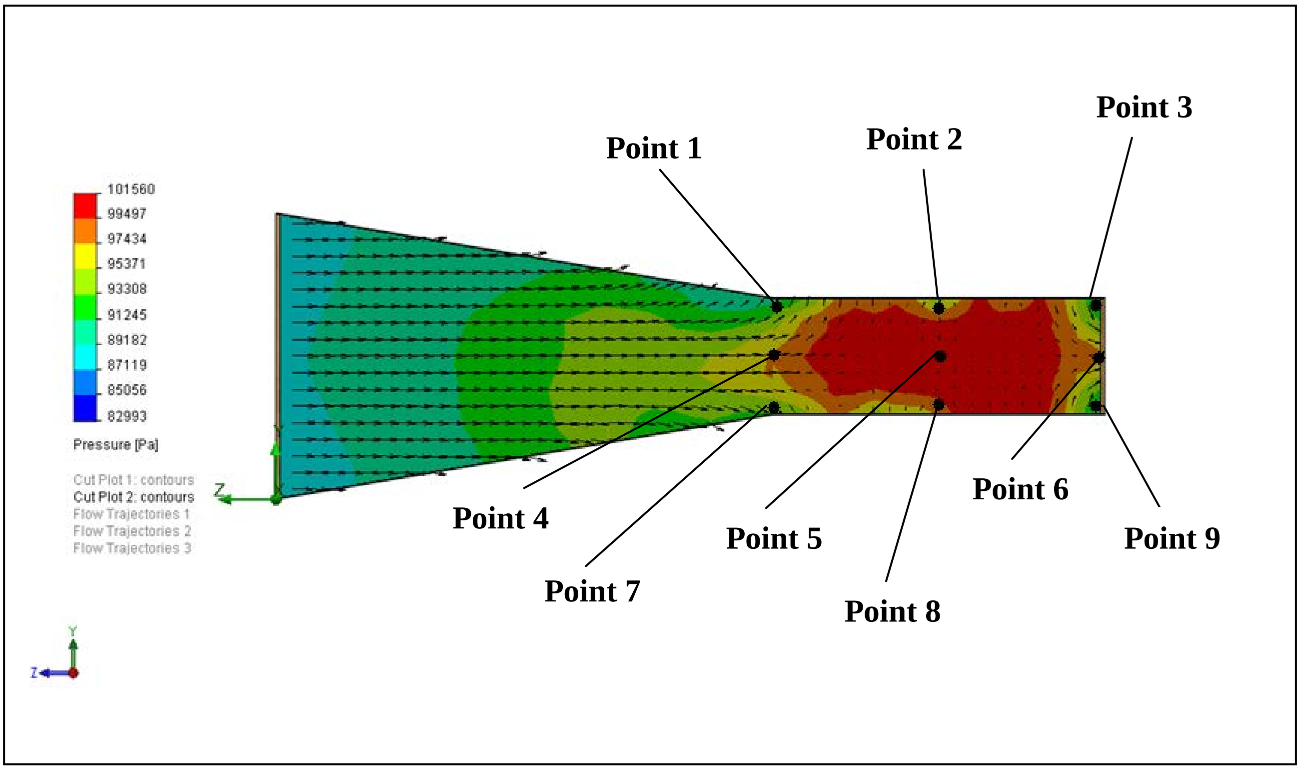

Figure 4.3: Pressure distribution points inside the testing chamber

This simulation testing is made to find out the effect of the contraction ratio towards the pressure distribution inside the testing chamber. From the simulation testing, all three cones are tested with 2.0 m/s initial air speed and the pressure distributions are measured at 9 different points inside the testing chamber as shown in Figure 4.3. The pressure distributions data is shown in Table 4.3. The pressure distributions are essential to be tested inside the testing chamber because if the pressure distributions are affected by the contraction ratio, then the results of model testing are also potentially affected.

Point	Pressure distributions, Pa		
	CR 6:1	CR 8:1	CR 9:1
1	93308	87349	101834
2	95371	97512	101834
3	91245	97512	97520
4	97434	87349	101834
5	99497	99544	101834
6	97434	97512	95363
7	93308	93447	101834
8	97434	97512	101834
9	91245	97512	99677

Table 4.3: The air flow pressure distributions inside every contracting cone

Table 4.3 shows the pressure distributions values at 9 different points inside the testing chamber for each cone. For further understanding, the pressure distributions can be represented as shown in Figure 4.4.

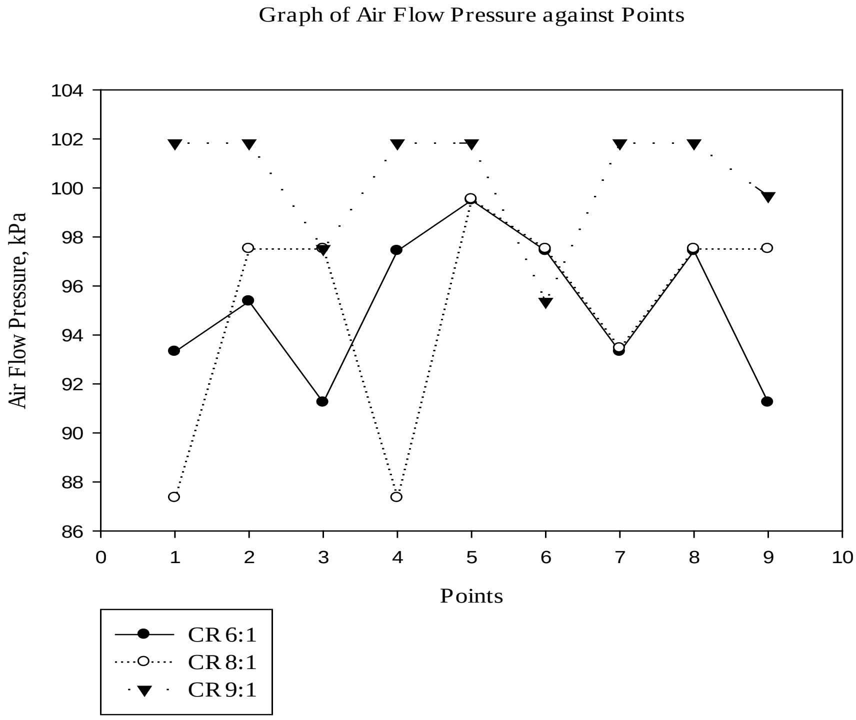

Figure 4.4: A graph of pressure distribution against points inside the testing chamber

Figure 4.4 shows the pressure distributions pattern inside the testing chamber for each contracting cone. The pressure distributions values are different for every testing chamber. However, the pressure distributions trend for 6:1 and 9:1 cones are about the same. For 6:1 cone, the highest pressure measurement is at Point 5 at about 99497 Pa while the lowest pressure measurements are at Point 3 and 9 approximately 91245 Pa. Point 5 is right at the center of the testing chamber while Point 3 and 9 are at the very exit of the testing chamber. For 8:1 cone, the pressure distributions trends are quite different from the other two cones. The highest pressure measurement is at Point 5 at about 99544 Pa while the lowest pressure measurement is at Point 1 and 4 at about 87349 Pa. Point 5 is in the middle of the testing chamber while Point 1 and 4 are at the entrance of the testing chamber. For 9:1 cone, pressure measurements are almost the same at every point and the values are higher than the other cones reading. The lowest measurement is at Point 6 at about 97520 Pa. The lowest pressure is at the exhaust of the testing chamber. From the graph, the trend of the pressure distribution inside the testing chamber can be concluded as the pressure is at the highest reading at the center area of the testing chamber because of the highest compression of air occurs at Point 5 meanwhile the lowest overall pressure measurement is at the exhaust area of the testing chamber because at that spot, the air is at the closest distance to the blower fan that forcing the air to flow out of the testing chamber with suction method.

After considering the simulation testing in order to select the contracting cone as the crucial design for the whole wind tunnel, a few factors have to be considered in order to pick one design of the contracting cone that is reliable and affordable. The first factor of cone selection is the speed regime that must satisfy the low-speed or a subsonic rule that is the air flow speed must below 0.3M approximately 100 m/s. For this rule, all of these three cones satisfied the subsonic rule that the highest air flow speed is only 6.7 m/s.

The second rule of selection is the construction cost. This rule defines that the larger ratio of the cone, the larger the cone size will be and more materials needed to build the cone. This might lead to higher construction cost. So, from these three cones, the one with 6:1 contraction ratio will be selected as it accomplished the both rule of cone selection. The 6:1 cone is the smallest in size due to smallest ratio and the air flow speed is not exceeding 100 m/s.

4.2.3 Honeycomb Effect

Honeycomb or flow straightener is a crucial part of the wind tunnel that have to be tested in flow simulation in order to investigate the effect of the honeycomb toward the flow speed and pressure inside the testing chamber. The results of the simulation testing are represented by the cutplot as shown in Figure 4.6.(a) and Figure 4.6.(b).

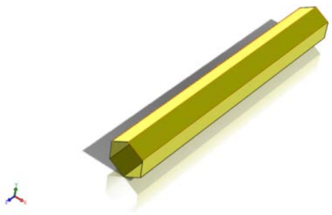

Figure 4.5: An isometric view of the designed honeycomb

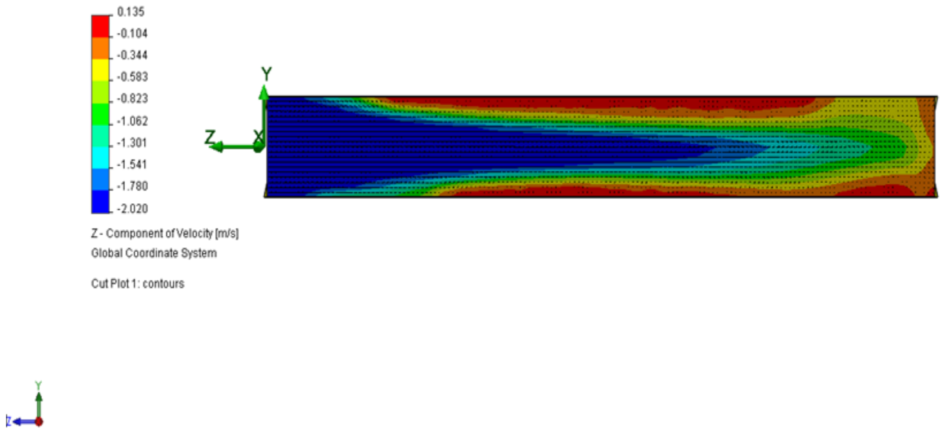

Figure 4.6.(a) : The velocity cutplot of the hexagonal honeycomb

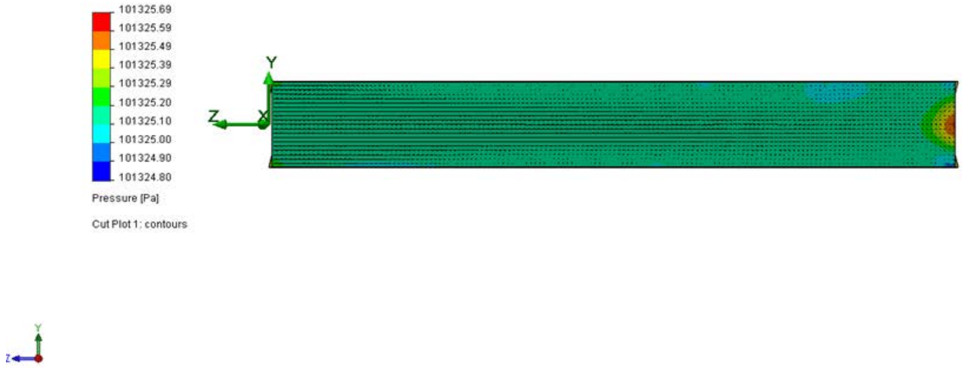

Figure 4.6.(b) : The Pressure cutplot of the hexagonal honeycomb

From the Figure 4.6.(a) through Figure 4.6.(b), the cutplots indicate that the honeycomb slightly affects the velocity and the pressure of the air flow that pass through the contracting cone to the testing chamber. The honeycomb is tested with 2.0 m/s air flow speed that was set to flow through it and the honeycomb dampens the air flow speed down to 0.583 m/s at the end of the duct. As for the pressure, the honeycomb only affect a little by increasing a bit of pressure at the end of the duct from 101325.20 Pa to 101325.49 Pa. So, for better designation, a bit more powerful suction fan is required to drive faster air into the testing chamber.

4.3 CALCULATION OF REYNOLD'S NUMBER

The calculation of Reynold's number is required to indicates whether the air flow is turbulence or laminar. In order to calculate the Reynold's number, the length of the model, L is represented by the overall length of the Ahmed Body for Ahmed Body analysis and the overall length of the cylinder model for the case study.

4.3.1 Reynold’s Number of Ahmed Body and Cylinder model

$$\text{Re} = \frac{\rho V L}{v} \tag{4.1}$$

By using the Reynold’s number equation as represented in Equation 4.1, both Reynold’s number for the Ahmed Body and cylinder model as shown in Table 4.4.

Model	Reynold’s Number
Ahmed Body	3.23×10^4
Cylinder Model	1.36×10^4

Table 4.4: Reynold’s Number for Ahmed Body and Cylinder model

The calculated Reynold’s number is low which is suitable for the tunnel dimension and the speed of the fan. Moreover, this number did not affect too much for the flow pattern characteristic. According to Vino et al., 2004, the changing of the Reynold’s number only affects the drag characteristic.

4.4 AHMED BODY ANALYSIS

In this part, the main model for this wind tunnel calibration, the Ahmed Body will be analysed experimentally and also by using Computational Fluid Dynamics (CFD).

4.4.1 Analysis on the front part

The analysis for the front part of Ahmed Body is only covered on the curved and entire top surface of the model. The characteristic of the instantaneous flow structure on the front part of the Ahmed Body can be described on Figure 4.7, as the smoke was pumped at the middle front of the model and the separation of the flow can be observed. The initial condition and size of the separated flow region is reducing along the consumption of time.

Figure 4.7: The position of the Ahmed Body before the experiment.

4.4.2 Analysis on the slant angle

Figure 4.8(a) shows the smoke was pumped at the centerline from the top view, while the flow pattern is shown in Figure 4.8(b). It indicates that the detached flow is observed from the leading edge of slant angle. It is also observed that the flow does not indicate any sign of reattachment at the middle of the slant surface but it appears that the flow is remains closed to the surface before the base.

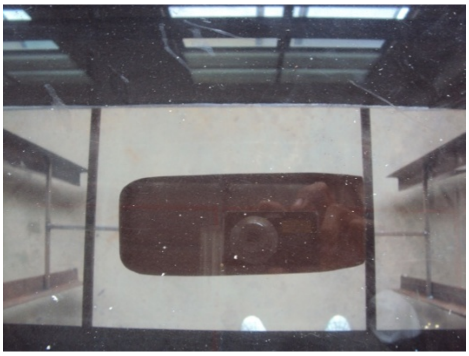

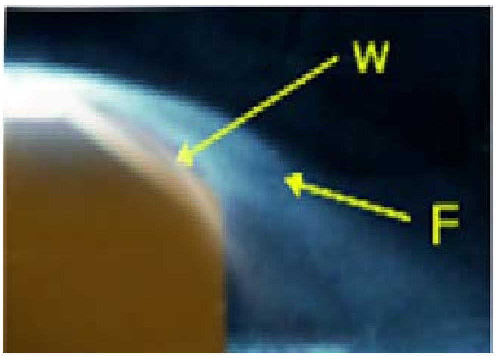

(a) Top view

(b) Side view

Figure 4.8: Smoke flow pattern at the slant surface and rear surface. a) Top view and, b) Side view of the test model in a testing chamber

In addition, there is no separating circulating flow that reattaches to the slant surface are observed in the separated flow region but only weak region of smoke is observed close to the body. This shows that this weak region of smoke is mixed with the flow separation region behind the vertical base.

This condition is very well visible in the simulation, where the weak of smoke region is shown in light blue and blue part shows the separated region flow. The figure also shows that the flow is separated at the leading edge of the slant surface with the weak region vacates into the separated region behind the vertical base.

There is some agreement with the previous works of (Vino et al., 2004), who also found that the detached flow region on the slant was no fully reattach but mixed with the large separation behind the vertical base. This agreement is supported by Spohn and Gillieron (2002), who used 25^{o} slant angle which promote reattachment also observed this condition. There is some contrast with Ahmed topology where state that large separation circulating flow is observed where the flow separate at the end of top surface and reattached again to the surface near vertical base before separating again at the base.

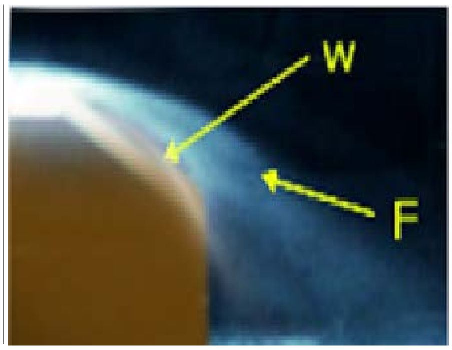

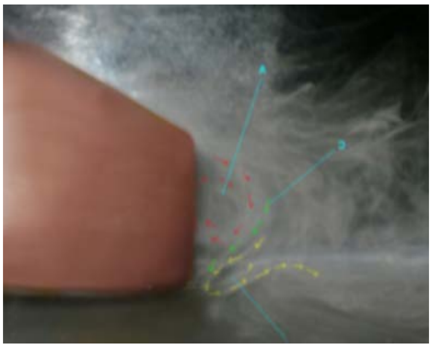

(a) (b)

Figure 4.9: (a) High drag flow structure and, (b) Low drag flow structure by experiment and flow trajectories.

Figure 4.9 shows the drag characteristic at the slant surface. This drag characteristic is determined by variable the Reynolds Number, first is using 2.0 m/s velocity of air as shown in Table 4.4.

From the experiment and simulation shows that drag is higher at low speed and gradually decrease with increasing Reynolds Number. This drag characteristic can be concluded that the slower the free stream speed, the longer that the low drag state is exist. This drag characteristic is shows good agreement with (Vino et al., 2004) who proposed that the drag characteristics are affected by change in Reynolds Number.

4.5 DISCUSSION ON AHMED BODY

From the flow pattern testing, it shows that the Ahmed Body smoke flow obeys the flow characteristic of the calibrated testing of Ahmed Body by Vino (2004). However, it is hard to obtain the desired flow pattern during the testing. There are several problems that might occur while conducting the wind tunnel testing that might affect the result of the flow pattern testing.

4.5.1 Smoke generator

The smoke generator generates its own flow velocity when the pump is pushing the smokes through the hose. Since the wind tunnel air flow is very slow, the smoke generator flow will slightly collides with the wind tunnel flow that eventually creates unsmooth flow form. It is the best to locate the smoke hose parallel with the wind tunnel flow direction.

4.5.2 Air gaps

The flow will be smooth if there is no air gap along the entrance to the testing chamber. If there is any gap, the outside air tends to flow into the testing chamber, interrupting the flow inside the testing chamber. To overcome this problem, the silicone sealant must be applied at the suspicious point at the wind tunnel to seal the air about each time to run the experiment.

4.5.3 Honeycomb alignment

The function of the honeycombs is to straighten the flow from the contracting cone. It is bad to run the experiment without proper alignment of the honeycomb because the honeycomb will be directing the flow to the wrong trajectory. To overcome this error, the honeycomb should be well aligned to ensure the right flow trajectory.

4.5.4 Summary

The flow pattern around the model is well defined in both experiment and simulation method. However, there are some significant disagreement between experimental and simulation results. In the experiment, the flow separates at the edge of slopping surface and reattach at the entire slant surface (but not fully reattach) after a few moment. In the simulation, the flow first stay attached before it separates somewhat downstream of the corner and it does not reattach again on the slant surface. This is due to coarse grids at the slant surface in the simulation technique.

4.6 CASE STUDY: CYLINDER MODEL ANALYSIS

4.6.1 Introduction

The result for Reynolds number, Re and coefficient of drag, Cd been obtained and will be analyzed here. The Reynolds number is use whether the condition for the experiment in turbulent or laminar.

Velocity, *V*, m/s	**Reynolds number, Re**	**Coefficient of drag, Cd**
2.0	8.8386×10^3	1.5

Table 4.5: Reynold's Number and drag coefficient for cylinder

The velocity of air is determined by using hot wire anemometer for each case study. Although the calculation shows that the Reynolds Number values are a bit low, it is considerably as turbulence due to model and tunnel size. Vino et al., 2004 stated that the changing of Reynolds Number only affects the drag characteristics. The drag characteristics are significantly decreased as the Reynolds Number increase.

4.6.2 Result

The result for the first case study has been obtained and will be analyzed in this section. Table 4.6 shows the summarized results from experiments with velocity of 0.6 m/s. There are three readings is taken for each points to determine the average height for whole experiment.

Point	**Height, H1, m**	**Height, $H_{2.1}$, m**	**Height, $H_{2.2}$, m**	**Height, $H_{2.3}$, m**	**Height, H_{avg}, m**	**Pressure difference, ΔP, Pa**	**Flow speed, *u*, m/s**
1	0.2900	0.2895	0.2920	0.2915	0.2910	0.01181124	0.1401
2	0.2900	0.2940	0.2940	0.2940	0.2940	0.0472450	0.2801
3	0.2900	0.2920	0.2915	0.2925	0.2920	0.02362248	0.1981
4	0.2900	0.2935	0.2920	0.2920	0.2925	0.0295281	0.2215
5	0.2900	0.2945	0.2940	0.2935	0.2940	0.0472450	0.2801
6	0.2900	0.2945	0.2960	0.2960	0.2955	0.0649618	0.3285
7	0.2900	0.2980	0.2980	0.2980	0.2980	0.0944899	0.3962
8	0.2900	0.3000	0.3000	0.2985	0.2995	0.1122068	0.4317

Table 4.6: Velocity at V = 2.0 m/s

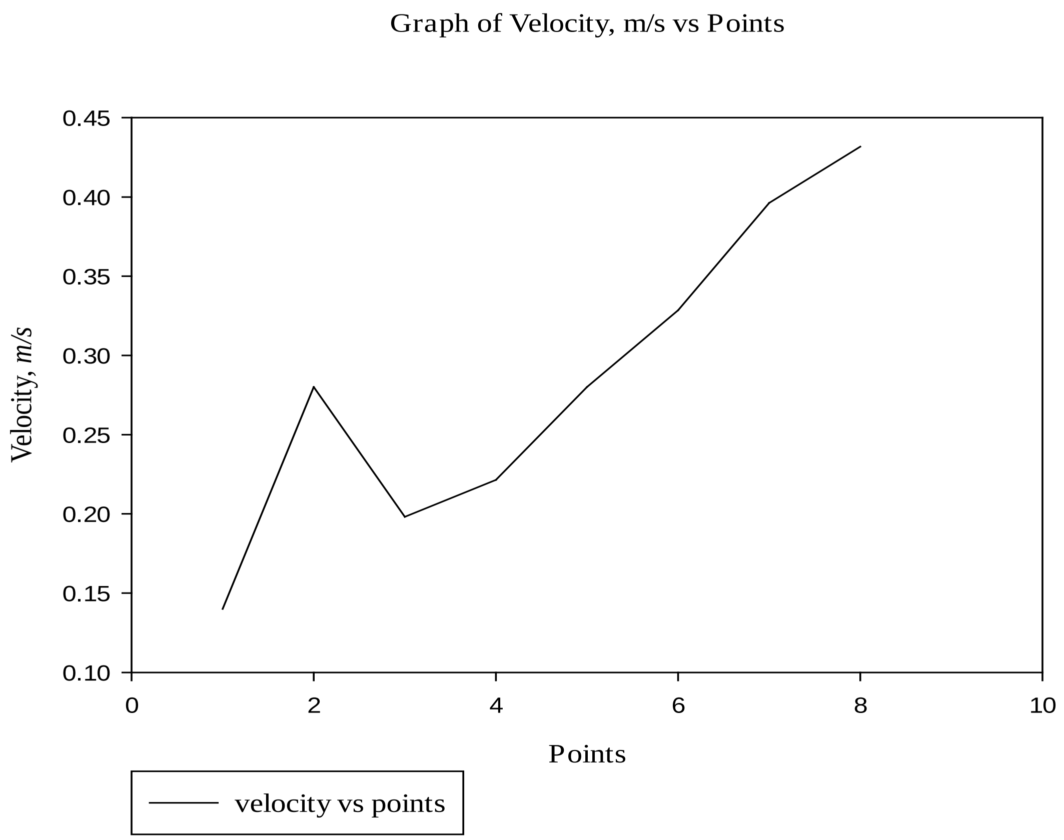

Figure 4.10: The graph of velocity, m/s versus the points at 2.0 m/s velocity of air flow.

From the Figure 4.10, the minimum value of flow speed is at point 1 for velocity at 2.0 m/s which is at 0.1401 m/s. For the maximum value of flow speed is at point 8 for velocity at 2.0 m/s which is at 0.4317 m/s. The value of differences between the velocity for minimum value of flow speed at 0.1401 m/s is three times the velocity of flow speed of 0.4317 m/s. This result occurred due to the turbulent flow over the streamlined body.

4.7 DISCUSSION ON CASE STUDY

The results that obtained are from the experiments are to be discussed in this section. The discussion part will cover the whole testing of the case study which is the cylinder model. From the experiment cylinder is considered bluff body because at large Reynolds numbers the drag is dominated by the pressure losses in the wake. The variation of the drag coefficient with Reynolds number is shown in Table 4.5, and the corresponding flow patterns are shown in chapter 3. The Reynolds number increases the variation in the drag coefficient and over a large range in Reynolds number it is nearly constant. Each point has its own velocity along the cylinder streamlines. But, the patterns from the results are actually different between the velocities of air through the object. The velocity increase or decrease is affected by the pressure different at each point whether at high speed or low speed. From the data taken, the end point is having higher pressure different. This means that the velocity at that point is higher than other point. Related to the bluff body, the dominant source of drag is pressure drag.

This test is a case study to study the pressure distribution along the cylinder's surface when the air flow was introduced to it. From Figure 4.9, the highest pressure is at point 8 at about 0.1122068 Pa, meanwhile, the lowest pressure is at point 1 at about 0.01181124 Pa. According to Bernoulli Principle, the flow velocity is inversely proportional to the pressure. But, in this study, after a few times of experimenting, the experimental value is slightly disobeying the principle. Several errors might have been occurred while conducting this experiment.

4.7.1 Wake region

Cylinder was selected in this experiment as a case study; unfortunately the cylinder generates a huge wake region after the air flow introduced to it. This wake region is a huge disturbance to have a good manometer reading. A further study of experimental method should be carried out in order to obtain any useful data for result calculation. Another suggestion is to change the test model to a more streamlined model to avoid from the wake region to be generated.

CHAPTER 5

CONCLUSION AND RECOMMEDATIONS

5.1 CONCLUSION

Generally, an open-loop low-speed wind tunnel was managed to be constructed with detail design justification and comprehensive analysis with the aid of the existing instrumentations available in the laboratory. The performance analysis on the small scale suction type open-loop low-speed wind tunnel have been managed to be conducted. Firstly, the flow pattern of vortex shedding around the Ahmed Body has been studied with observing the flow patterns using the small scale model that indicates there is no differences with the original scale model that proposed by the model founder. Moreover, from the experiment, the flow patterns observed has a good agreement with the tested Ahmed Body in the calibrated wind tunnel. According to the performance evaluation of the cylinder model, the minimum value of flow speed is at point 1 which the value of air velocity is 2.0 m/s that give 0.1401 m/s of flow speed. Meanwhile at the point 8, the air velocity is the highest at 2.0 m/s which is at 0.4317 m/s of flow speed. However, the result is not obtained at its best condition as there is wake flow occurred over the cylinder body.

5.2 RECOMMENDATIONS

Based on the aspect of design, fabrication, and performance testing of the wind tunnel, several considerations should be improved in order to obtain better result for performance testing and also to ensure a better resistance of the wind tunnel itself for a longer lasting wind tunnel life.

5.2.1 Change the material

For better durability of the wind tunnel, several reconstructions of the wooden parts with more tough material such as aluminum sheets or the Perspex should be done. The contraction cone and the diffuser are built from the wood because it is cheap and easy to be joined together. However, after a few testing, the strength of the wooden part can be doubted as is starts to sway when the surrounding air in contact with it.

5.2.2 Change the fan

In order to carry out the experiment of the effect out various air velocities, a fan with a higher speed is necessary to be considered in the wind tunnel construction. The current fan is only at about 30W and only can generate only a level of air velocity which is at about 2.0 m/s. There are more results of studies can be obtained with various speed of the air velocity.

5.2.3 Portability

The current wind tunnel is quite huge that required quite a space in the laboratory, In order to have better portability, the parts should have the ability to be disassembled and easier to be stored.

5.2.4 Adjustable cone

As for further development for the studies of relation between the contraction ratio and the generated flow speed, an adjustable contracting cone in the range of 1:6 to 1:9 is necessary to be considered in the wind tunnel construction. In this way, people will be able to study the actual effect of the contraction ratio to the generated intake air flow that will definitely give changes on the result of the tested model.

REFERENCES

Aref, H., Stremler M.A., Ponta F.L. 2006. Exotic vortex wakes—point vortex solutions. Journal of Fluids and Structures, Volume 22, Issues 6-7, Pages 929-940. Elsevier Ltd.

Akbari, M.H. 1999. Bluff-body Flow Simulations Using Vortex Methods. Ph.D Thesis. McGill University Montreal, Canada.

Arbey H, Bataille J. Noise generated by airfoil profiles placed in a uniform laminar flow. JFM 1983;134:33–47.

Azlan, D. 2006. Design Analysis and Fabricate Small Open Low Speed Wind Tunnel. Degree Thesis. University Malaysia Pahang, Malaysia: November 2006.

Chi-fu W. and Williams. J. 2005. Design, Construction and Testing an Educational Subsonic Wind Tunnel.

Cogotti, A., 2000. Flow field measurements and their interpretation. Euromotor International Short Course on Vehicle Aerodynamics, Stuttgart, February 2000.

Gabbai, R.D, Benaroya H. 2004. An overview of modeling and experiments of vortex-induced vibration of circular cylinders. Journal of Sound and Vibration 282 (2005) 575–616. Elsevier Ltd.

Hinterberger, C., Villalba, M.G., and Rodi, W. 2002. Large eddy simulation of flow around the Ahmed body. In McCallen R., Browand F., Ross J. (Eds.) The Aerodynamics of Heavy Vehicles: Trucks, Buses, and Trains. California : Springer.

Irwin P.A. 2007. Bluff Body Aerodynamics in Wind Engineering. Journal of Wind Engineering and Industrial Aerodynamics. Elsevier Ltd.

Leclercq D, Doolan C, Reichl J. Development and validation of a small-scale anechoic wind tunnel. In: 14th international congress on sound and vibration, Cairns, Australia; 2007.

Liu, Y. & Moser, A. 2003. Numerical modeling of airflow over the Ahmed body. Proceedings of the 11th Annual Conference of the CFD Society of Canada, V2,P507-512,2003. Swiss Federal Institute of Technology, Zurich, Switzerland.

Mathew, J. 2006. Design, fabrication, and characterization of an anechoic wind tunnel facility. Ph.D Thesis. University of Florida. UMI reference number: 3224582.

Meneghini, J.R., Saltara, F., Fregonesi, R.A.& Yamamoto C.T. 2002. Vortex Induced Vibration on Flexible Cylinder. In: Chakrabart S. K. Numerical Models in Fluid-Structure Interaction. WIT press.

Nebres, Villafranca, J.L. 1992. Wake Similarity and Vortex Formation for Two-Dimensional Bluff Bodies. Ph.D Thesis. University of Notre Dame, Indiana.

Rae, William H. and Allan P., (1984), Low-Speed Wind Tunnel Testing, 2nd Edition, John Wiley and Sons Inc., Canada.

Rodi, W. 2004. DNS and LES of some engineering flows. Fluid Dynamics Research 38 (2006) 145–173. The Japan Society of Fluid Mechanics and Elsevier B.V.

Schatzman, J.C. 1981. A model for the Von Kármán Vortex Street. Ph.D Thesis. California Institute of Technology Pesadena, California, U.S.A: May 1981.

S.R Ahmed, R. Ramm and G.R. Faltin “Some salient features of the time averaged ground vehicle wake”, SAE Paper, 840300 (1995), 1–30.

Vino, G., Watkins, S., Mousley, P., Watmuff, J., Prasad S. 2004. Flow structures in the near-wake of the Ahmed model. Journal of Fluids and Structures 20 (2005) 673–695. Elsevier Ltd.

Williams, R.G.S. 2002. The Effect of Neighbouring Bodies on the Vortex-Excited Response of a Structure. Ph.D Thesis. University of Miami, U.S.A. UMI reference number: 3050753.

Würz W. Vetter C. Wind Tunnel Measurements of the LM NACA 64-618 Airfoil. . 2006 Report, IAG Universität Stuttgart.

APPENDIX

APPENDIX A: ISOMETRIC VIEW OF THE WIND TUNNEL

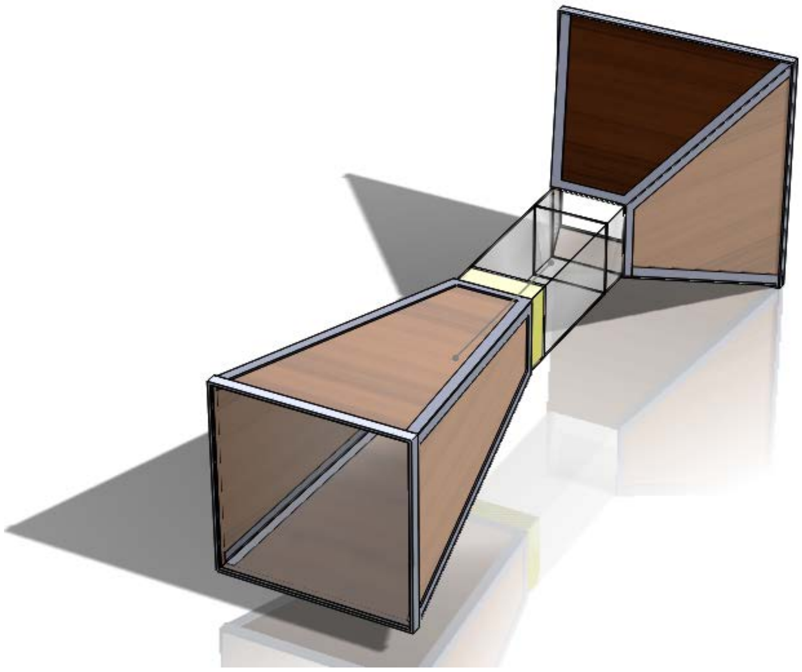

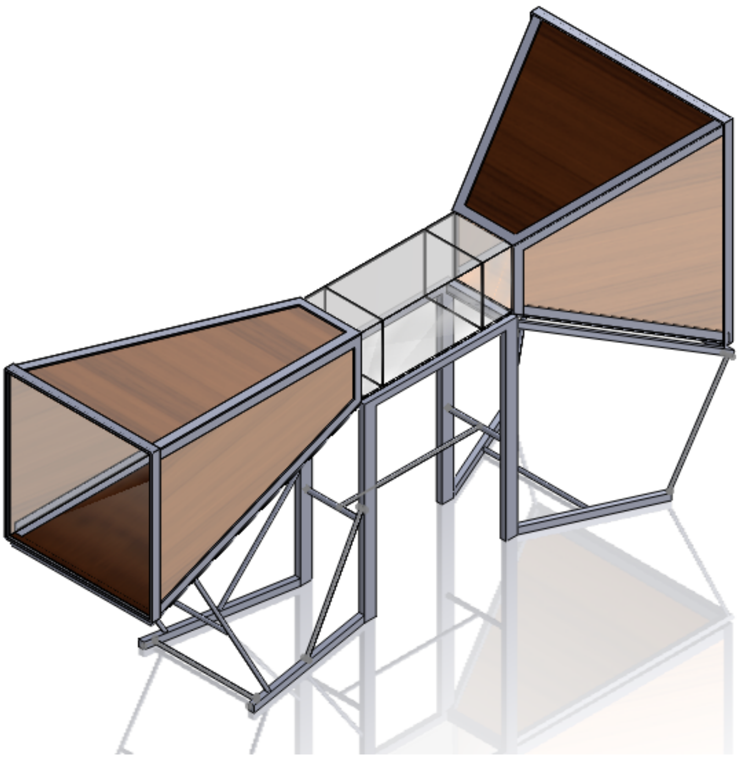

APPENDIX B: WIND TUNNEL WITH DIMENSION